References

[1] David Max, Richard S. Wallace: Feedback Control of Miniature Direct Drive Devices. Technical Report No. 652, Department of Computer Science, Courant Institute of Mathematical Sciences, New York University, 1993

[2] Richard S. Wallace: Miniature Direct Drive Rotary Actuators II: Eye, Finger and Leg. Technical Report No. 651, Department of Computer Science, Courant Institute of Mathematical Sciences, New York University, 1993

[3] John J. Craig: Introduction to Robotics, Mechanics and Control 2nd Edition. Addison-Wesley Publishing Company, Inc. ISBN 0-201-09528-9, 1989

[4] Il'ja N. Bronstein, Konstantin A. Semendjajew: Taschenbuch der Mathematik. Verlag Harri Deutsch, Thun. ISBN 3-87144-492-8, 1989

[5] Matthew T. Mason, J. Kenneth Salisbury, Jr.: Robot Hands and the Mechanics of Manipulation. The MIT Press, 1985

[6] National Semiconductor, LMD 18201 3A, 55V H-Bridge Data Sheet

[7] Pietro Buttolo, Dal-Yeon Hwang, Pierre-Henry Marbot, Blake Hannaford: Experimental Characterization of Hard Disk Actuators for Mini Robotics, IEEE Intl. Conference on Robotics and Automation, San Diego, 1994

[8] Richard S. Wallace: Scaling Direct Drive Actuators, Technical Report No. XXX, Department of Computer Science, Courant Institute of Mathematical Sciences, New York University, 1994

[9] Phillip John McKerrow: Introduction to Robotics. Addison-Wesley Publishing Company, Inc. ISBN 0-201-18240-8, 1991

[10] Chae H. An, Christopher G. Atkeson, John M. Hollerbach: Model-based control of a robot manipulator. The MIT Press, ISBN 0-262-01102-6, 1988

[11] John M. Hollerbach, Ian W. Hunter, John Ballantyne: A Comparative Analysis of Actuator Technologies for Robotics. The Robotics Review 2, Oussama Khatib, John J. Craig, Tomás Lozano-Pérez (eds.) The MIT Press, ISBN 0-262-11171-3, 1992

[12] George A. Bekey, Rajko Tomovic, Ilija Zeljkovic: Control Architecture for the Belgrade/USC Hand. Dextrous Robot Hands, S.T. Venkataraman, T. Iberall (eds.) Springer Verlag, ISBN 0-387-97190-4, 1990

h_{Ti}	height of connection tube part of link i
h_{Ci}	height of one coil of link i
a_i	length of side of coil in y-direction of link i
	attention: a_i has double meaning
b_i	length of side of coil in z-direction of link i
d_i	distance between two coils of link i
l_i	position of center of coils of link i
m_{Mi}	mass of magnet part of link i
m_{Ti}	mass of connection tube part of link i
m_{Ci}	mass of one coil of link i
r_{C_i}	position of center of mass of link i along X axis from origin of frame $\{i\}$
m_i	mass of link i
I_i	modeled inertia matrix of link i
$\{C_i\}$	frame with origin at the center of mass of link i and same orientation as frame $\{i\}$
k	kinetic energy of one finger
k_i	kinetic energy of link i
u	potential energy of one finger
u_i	potential energy of link i
g	gravity vector
P_i	position of frame $\{i\}$
K_T	torque constant
K_M	motor constant
$M(\theta)$	inertial matrix
$V(\theta, \dot{\theta})$	coriolis and centripetal torques
$G(\theta)$	gravitational torques
θ_d	desired position
$\dot{\theta}_d$	desired velocity
$\ddot{\theta}_d$	desired acceleration
θ	position measured with hall sensors
$\dot{\theta}$	velocity computed from sampled position data
K_p	3×3 matrix with position gains k_p
K_v	3×3 matrix with velocity gains k_v

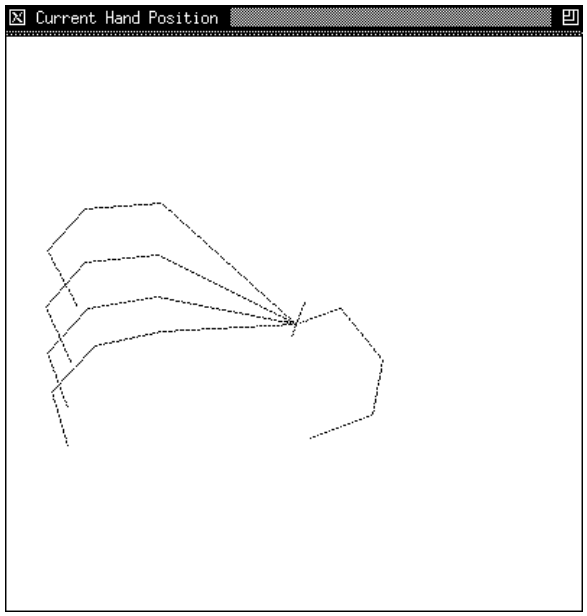

Figure 33: Direct drive hand graphics interface picture 3

d_i	distance from $\hat{X}_{i-1}$ to $\hat{X}_i$ measured along $\hat{Z}_i$
θ_i	angle between $\hat{X}_{i-1}$ and $\hat{X}_i$ measured about $\hat{Z}_i$
$\{F_j\} = \{0\}$	finger base frame
$\{0\} \ldots \{3\}$	finger link frames
$\{T\} = \{3\}$	tool frame (fingertip)
P	palm base frame
f	matrix composed of vectors that describe the position of the frames $\{F_j\}$ in relation to the frame P
φ_i	actuator angles $(0° \ldots 90°)$
α	frame angle θ_i to actuator angle φ_i conversion factor
R_i	intermediate frame for forward kinematics
P_i	intermediate frame for forward kinematics
x_T	x coordinate of fingertip
y_T	x coordinate of fingertip
γ	angle between the X axis of the fingertip and the X axis of the palm
v_i	linear velocity of frame $\{i\}$
w_i	angular velocity of frame $\{i\}$
I_M	inertia matrix of magnet part of link
I_T	inertia matrix of connection tube part of link
I_{2C}	inertia matrix of 2 coils
r_{Mi}	radius of magnet part of link i
h_{Mi}	height of magnet part of link i
r_{Ti}	radius of connection tube part of link i

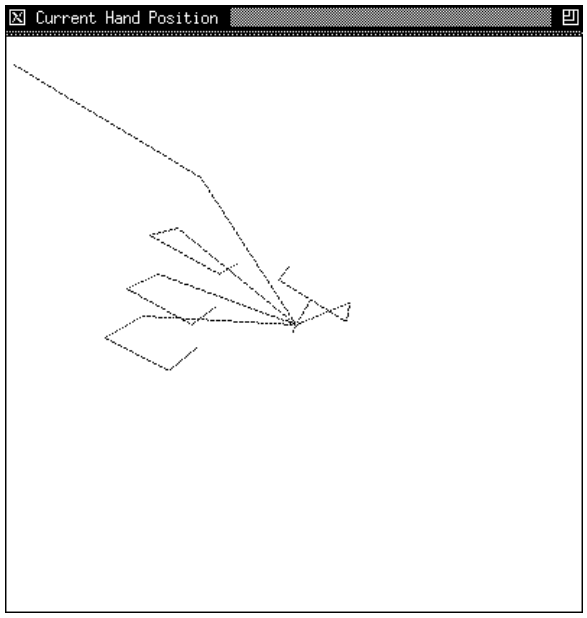

Figure 31: Direct drive hand graphics interface picture 1

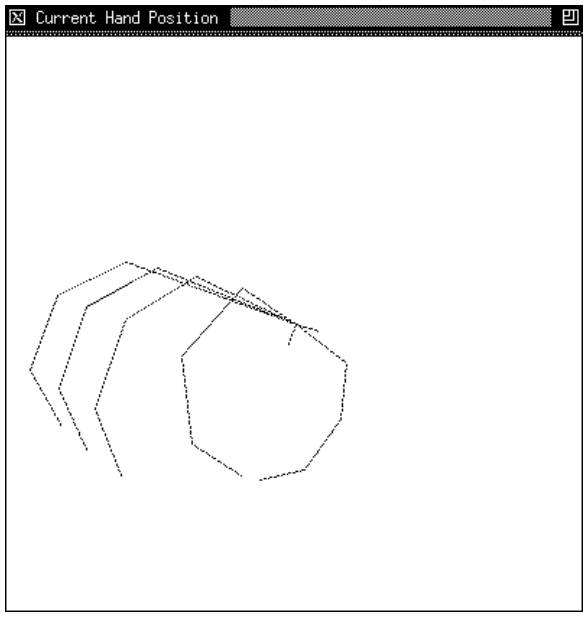

Figure 32: Direct drive hand graphics interface picture 2

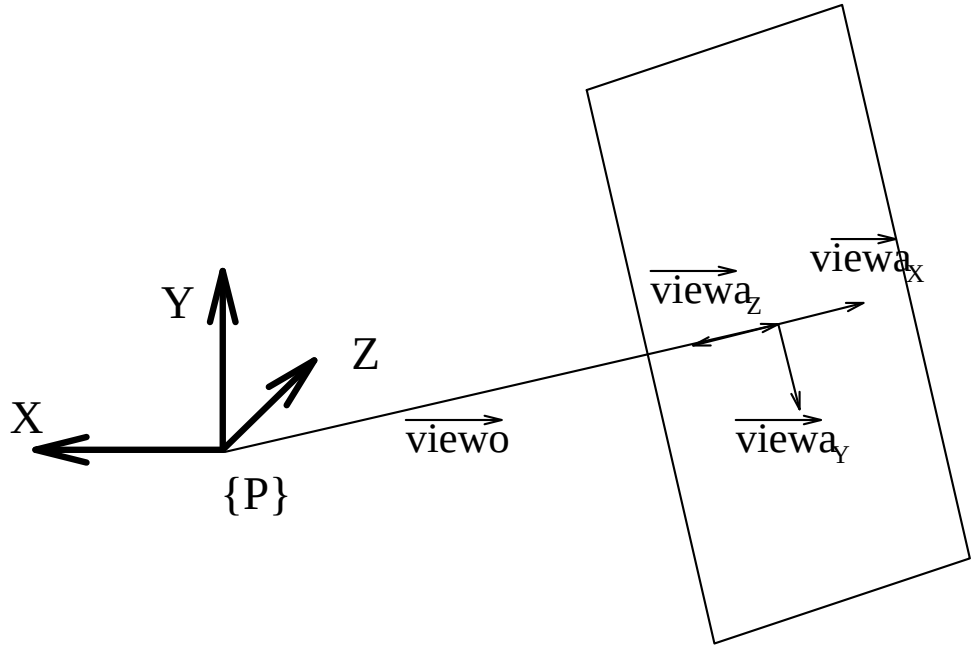

Figure 30: Direct drive hand graphics interface: View screen orientation

The orientation of the view screen relative to the hand is shown in Figure 30. The picture also visualizes how the rotation of the view screen works.

The direct drive hand interface can be used to grasp an object manually by adjusting the angles at each link. Also it is possible to place the hand in a certain configuration without an object. The screen visualizes where the position of the hand is according to the calculations. Due to compliance this position may be different from what the position of the real hand is. Thus we have a tool for the development of grasping algorithms and can verify how they work in theory and how they live up to their expectations in practice.

G List of variables and declarations

$\hat{X}_i$	unit vector that points along the perpendicular between $\hat{Z}_i$ and $\hat{Z}_{i+1}$ from link 1 to link i+1
$\hat{Y}_i$	unit vector that is derived from link $\hat{X}_i$ and $\hat{Z}_i$ according to the right hand rule
$\hat{Z}_i$	unit vector that points along the joint axis i
a_i	distance from $\hat{Z}_i$ to $\hat{Z}_{i+1}$ measured along $\hat{X}_i$ attention: a_i has double meaning
α_i	angle between $\hat{Z}_i$ and $\hat{Z}_{i+1}$ measured about $\hat{X}_i$

- **Close Hand** Closes the hand completely ($\varphi_i = 90°$ for all links and fingers)
- **Point Finger** The hand points at something with finger number 2.
- **Count 1** Extend finger number 1. All others are closed.
- **Count 2** Extend finger number 1,2. All others are closed.
- **Count 3** Extend finger number 1,2,3. All others are closed.
- **Count 4** Extend finger number 1,2,3,4. Finger 5 is closed.
- **Count 5** Extend finger number 1,2,3,4,5 (same as Open Hand).

To control the hand the following data can be entered:

- **L1:, L2:, L3:** θ_i for all fingers and links 1 through 3.
- **X:, Y:** x, y planar coordinates for all fingers.
- **gamma:** γ orientation of the fingertip.
- **tf:** t_f time to complete trajectory.
- **kp1:, kp2:, kp3:** k_p position gains.
- **kv1:, kv2:, kv3:** k_v velocity gains.
- **gx:, gy:, gz:** g gravity vector for palm of hand.
- **et:, ea:, ev:, ep:** e_τ, e_a, e_v, e_p maximum errors for simulation of torque, acceleration, velocity and position.
- **Postscript Filename:** Sets the filename onto which the graph with the required current for finger 2 (link 1 through 3) is written during simulation. A graph will only be written during simulation if a filename is set.
- **Maximum Current for Graph:** Sets the maximum current that will be shown on the graph.

The following data is displayed by the DDHGI:

- **IM1:, IM2:, IM3:** I_{max1},I_{max2},I_{max3} maximum currents that occured during the trajectory for all fingers and links 1 through 3.
- **Z:** z coordinates for all fingers.

F.2 DDHGI Features

The following buttons are provided by the direct drive hand graphics interface:

- **Quit** The program will be terminated if the user presses this button.
- **Simulation** Once this button is pressed the trajectory for all links are calculated and the control algorithm can move the hand according to this trajectory. The starting points for the trajectories are the actual hand positions. Endpoints of the trajectory are derived according to the following rule. Whenever an angle of the hand is changed the program remembers this fact and sets the endpoint of the trajectory according to the joint angles. When the Cartesian coordinates are changed, this too is remembered and the endpoints are set accordingly. If both are changed precedence is given to the joint angles. The length of the trajectory is determined by the final time that can be set individually for all fingers. If a final time of 0 is set then no trajectory will be calculated and the simulated hand will be moved instantly to its new position.
- **Perspective** The hand can be viewed with and without perspective. This button toggles the perspective mode on or off.
- **Move Horizon In** The position of the horizon moves closer to the view screen by a preset amount.
- **Move Horizon Out** The position of the horizon moves away from the view screen by a preset amount.
- **Move In** Zooms in on the hand.
- **Move Out** Zooms out from the hand.
- **Rot X Right** Rotates the origin of the view screen around the X axis to the right.
- **Rot X Left** Rotates the origin of the view screen around the X axis to the left.
- **Rot Y Right** Rotates the origin of the view screen around the Y axis to the right.
- **Rot Y Left** Rotates the origin of the view screen around the Y axis to the left.
- **Rot Z Right** Rotates the origin of the view screen around the Z axis to the right.
- **Rot Z Left** Rotates the origin of the view screen around the Z axis to the left.
- **Home** The view screen returns to its home (original) position.
- **Open Hand** Opens the hand completely ($\varphi_i = 0°$ for all links and fingers)

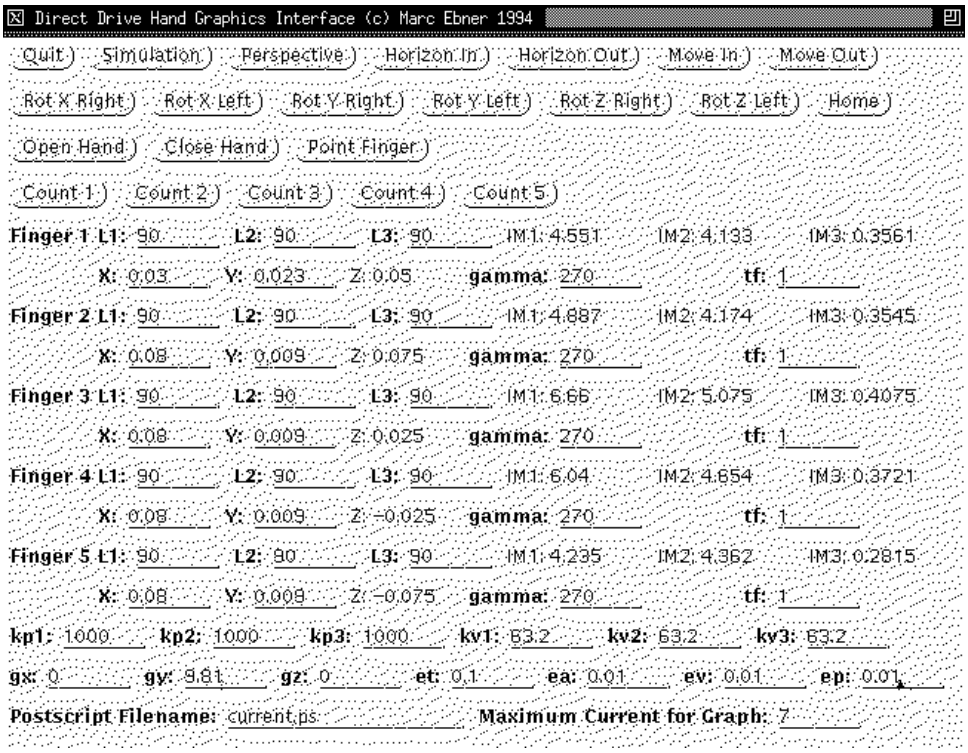

Figure 28: Direct drive hand graphics interface: control panel

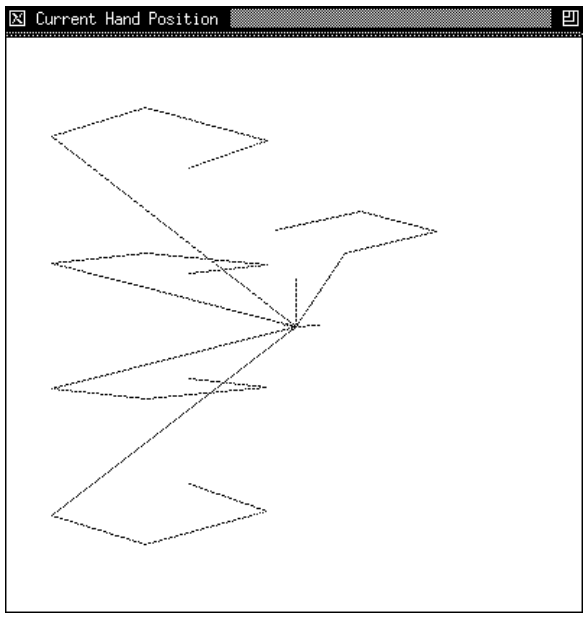

Figure 29: Direct drive hand graphics interface: view screen

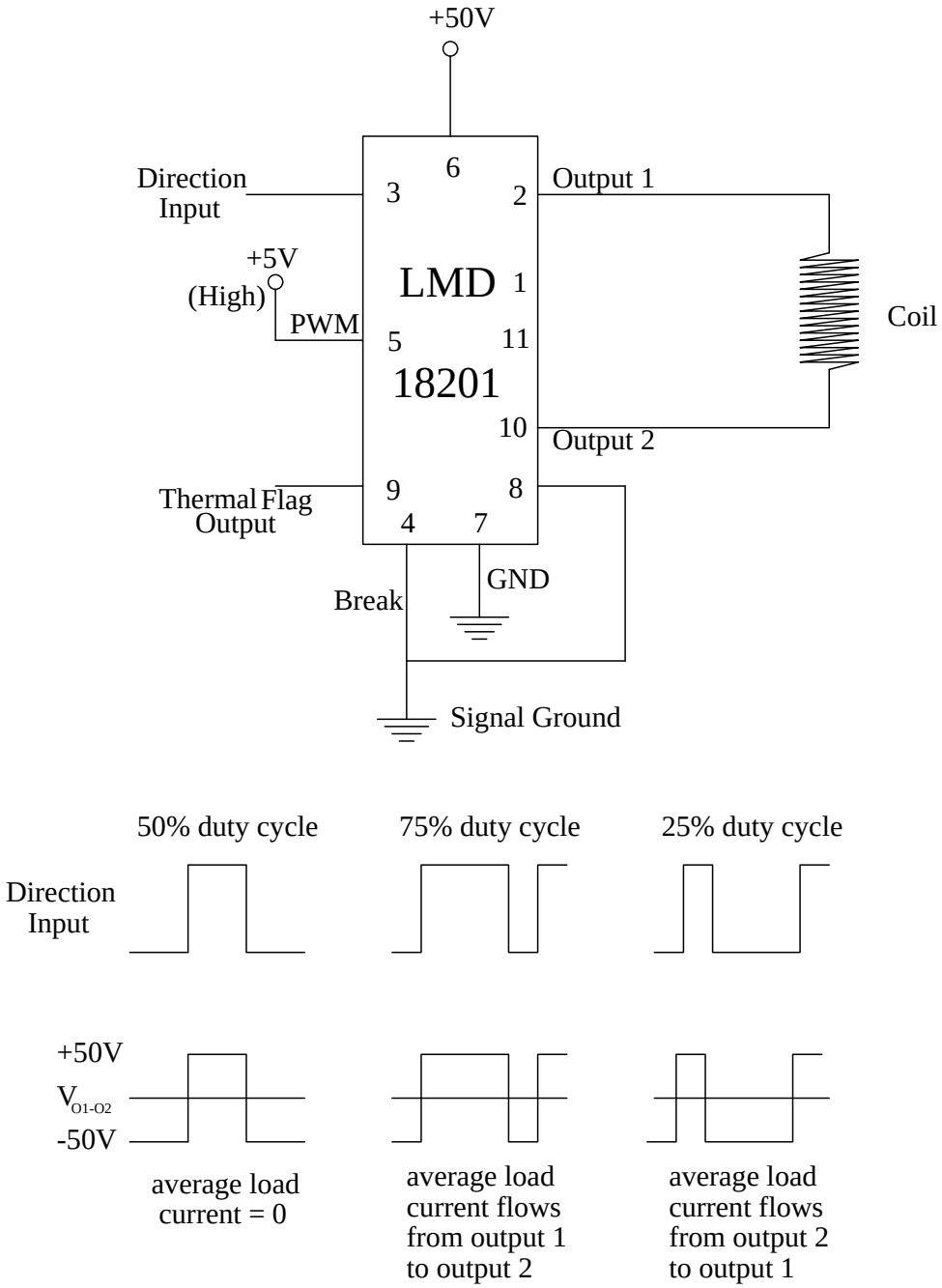

Figure 27: LMD 18201 3A, 55V, H-Bridge

E Control circuit

The control circuit that will be used to supply current to the coils is shown in Figure 27. Pin 5 controls the amount of current supplied to the coils via pulse width modulation. The current is proportional to the duty cycle of the signal at pin 5.

F Direct drive hand graphics interface

The Direct drive hand graphics interface (DDHGI) was developed specifically for the direct drive hand. It simulates the movement of the hand and can be upgraded to include control of the actual hand once the control hardware is completed and the Hall sensors are included into the hand. It provides a tool for checking different control algorithms and estimation of maximum current requirements.

F.1 DDHGI Windows

The DDHGI consists of two windows:

- the control panel (Figure 28)

  The control panel gives the user the means to control the position of the view screen relative to the hand position as well as the means to control the position of the hand itself. The user can control each individual joint of the hand by entering the desired angle and pressing the Simulation button. Buttons to move the hand into a number of preset positions (e.g. open hand, close hand, point finger) are also provided. Furthermore we can change the physical orientation of the hand in space by varying the gravity vector. The characteristics of the control algorithm can be changed by entering different position and velocity gains. The maximum error that is introduced to torque, acceleration, velocity and position can also be changed.

- the view screen (Figure 29)

  The view screen shows the current position of the hand. The hand position is drawn schematically. Each finger is shown by drawing a line from the origin to its knuckles, from the knuckles to the first link, from the first link to the second, from the second to the third and finally, from the third link to the fingertip. This provides all the necessary information and provides and easy method to check for accurate control if the hand is viewed sideways without perspective. The X axis of each link is in the direction of the line going from one link to the next, or from the final link to the finger tip. The Z axis is along the axis of rotation of each link and the Y axis is perpendicular to both the X and Z axis.

$$
\begin{aligned}
&= \begin{bmatrix} -a_1 s_1 \dot{\theta}_1 - a_2 s_{12}(\dot{\theta}_1 + \dot{\theta}_2) \\ a_1 c_1 \dot{\theta}_1 + a_2 c_{12}(\dot{\theta}_1 + \dot{\theta}_2) \\ 0 \end{bmatrix} \\
{}^0v_T &= {}^0_3R \cdot {}^T v_T = \begin{pmatrix} c_{123} & -s_{123} & 0 \\ s_{123} & c_{123} & 0 \\ 0 & 0 & 1 \end{pmatrix} \cdot \begin{bmatrix} a_1 s_{23}\dot{\theta}_1 + a_2 s_3(\dot{\theta}_1 + \dot{\theta}_2) \\ a_1 c_{23}\dot{\theta}_1 + a_2 c_3(\dot{\theta}_1 + \dot{\theta}_2) + a_3(\dot{\theta}_1 + \dot{\theta}_2 + \dot{\theta}_3) \\ 0 \end{bmatrix} \\
&= \begin{bmatrix} -a_1 s_1 \dot{\theta}_1 - a_2 s_{12}(\dot{\theta}_1 + \dot{\theta}_2) - a_3 s_{123}(\dot{\theta}_1 + \dot{\theta}_2 + \dot{\theta}_3) \\ a_1 c_1 \dot{\theta}_1 + a_2 c_{12}(\dot{\theta}_1 + \dot{\theta}_2) + a_3 c_{123}(\dot{\theta}_1 + \dot{\theta}_2 + \dot{\theta}_3) \\ 0 \end{bmatrix}
\end{aligned}
$$

D.2 Jacobian

The Jacobian transforms the joint velocities $\dot{\theta}$ to the linear and rotational velocities.

$$
{}^0V = \begin{bmatrix} {}^0v \\ {}^0w \end{bmatrix} = {}^0J(\theta)\dot{\theta}
$$

Since each finger is a planar manipulator we only need to consider the linear velocity vector.

$$
\begin{aligned}
{}^T v_T &= {}^T J(\theta)\dot{\theta} \\
&= \begin{pmatrix} a_1 s_{23} + a_2 s_3 & a_2 s_3 & 0 \\ a_1 c_{23} + a_2 c_3 + a_3 & a_2 c_3 + a_3 & a_3 \\ 0 & 0 & 0 \end{pmatrix} \cdot \begin{bmatrix} \dot{\theta}_1 \\ \dot{\theta}_2 \\ \dot{\theta}_3 \end{bmatrix}
\end{aligned}
$$

For the Jacobian in the frame $\{0\}$ we get:

$$
\begin{aligned}
{}^0J(\theta) &= {}^0_3R \cdot {}^T J(\theta) = \begin{pmatrix} c_{123} & -s_{123} & 0 \\ s_{123} & c_{123} & 0 \\ 0 & 0 & 1 \end{pmatrix} \cdot \begin{pmatrix} a_1 s_{23} + a_2 s_3 & a_2 s_3 & 0 \\ a_1 c_{23} + a_2 c_3 + a_3 & a_2 c_3 + a_3 & a_3 \\ 0 & 0 & 0 \end{pmatrix} \\
&= \begin{pmatrix} -a_1 s_1 - a_2 s_{12} - a_3 s_{123} & -a_2 s_{12} - a_3 s_{123} & -a_3 s_{123} \\ a_1 c_1 + a_2 c_{12} + a_3 c_{123} & a_2 c_{12} + a_3 c_{123} & a_3 c_{123} \\ 0 & 0 & 0 \end{pmatrix}
\end{aligned}
$$

D.3 Static forces

To exert a static force ${}^0F_T$ at the fingertip we can use the transpose of the Jacobian to calculate the required torque at each joint.

$$
\begin{aligned}
\tau &= {}^0J^T \cdot {}^0F_T \\
&= \begin{pmatrix} -a_1 s_1 - a_2 s_{12} - a_3 s_{123} & a_1 c_1 + a_2 c_{12} + a_3 c_{123} & 0 \\ -a_2 s_{12} - a_3 s_{123} & a_2 c_{12} + a_3 c_{123} & 0 \\ -a_3 s_{123} & a_3 c_{123} & 0 \end{pmatrix} \cdot \begin{bmatrix} f_x \\ f_y \\ 0 \end{bmatrix}
\end{aligned}
$$

$$
\begin{aligned}
{}^1v_1 &= \begin{bmatrix} 0 \\ 0 \\ 0 \end{bmatrix} \qquad {}^1w_1 = \begin{bmatrix} 0 \\ 0 \\ \dot{\theta}_1 \end{bmatrix} \\
{}^2v_2 &= \begin{pmatrix} c_2 & s_2 & 0 \\ -s_2 & c_2 & 0 \\ 0 & 0 & 0 \end{pmatrix} \cdot \begin{bmatrix} 0 \\ a_1\dot{\theta}_1 \\ 0 \end{bmatrix} = \begin{bmatrix} a_1 s_2 \dot{\theta}_1 \\ a_1 c_2 \dot{\theta}_1 \\ 0 \end{bmatrix} \\
{}^2w_2 &= \begin{bmatrix} 0 \\ 0 \\ \dot{\theta}_1 + \dot{\theta}_2 \end{bmatrix} \\
{}^3v_3 &= \begin{pmatrix} c_3 & s_3 & 0 \\ -s_3 & c_3 & 0 \\ 0 & 0 & 1 \end{pmatrix} \left(\begin{bmatrix} a_1 s_2 \dot{\theta}_1 \\ a_1 c_2 \theta_1 \\ 0 \end{bmatrix} + \begin{bmatrix} 0 \\ 0 \\ \dot{\theta}_1 + \dot{\theta}_2 \end{bmatrix} \times \begin{bmatrix} a_2 \\ 0 \\ 0 \end{bmatrix} \right) \\
&= \begin{bmatrix} a_1 s_{23} \dot{\theta}_1 + a_2 s_3 (\dot{\theta}_1 + \dot{\theta}_2) \\ a_1 c_{23} \dot{\theta}_1 + a_2 c_3 (\dot{\theta}_1 + \dot{\theta}_2) \\ 0 \end{bmatrix} \\
{}^3w_3 &= \begin{bmatrix} 0 \\ 0 \\ \dot{\theta}_1 + \dot{\theta}_2 + \dot{\theta}_3 \end{bmatrix}
\end{aligned}
$$

Finally the velocity of the tool frame (the fingertip) is given by:

$$
\begin{aligned}
{}^Tv_T &= \begin{bmatrix} a_1 s_{23} \dot{\theta}_1 + a_2 s_3 (\dot{\theta}_1 + \dot{\theta}_2) \\ a_1 c_{23} \dot{\theta}_1 + a_2 c_3 (\dot{\theta}_1 + \dot{\theta}_2) \\ 0 \end{bmatrix} + \begin{bmatrix} 0 \\ 0 \\ \dot{\theta}_1 + \dot{\theta}_2 + \dot{\theta}_3 \end{bmatrix} \times \begin{bmatrix} a_3 \\ 0 \\ 0 \end{bmatrix} \\
&= \begin{bmatrix} a_1 s_{23} \dot{\theta}_1 + a_2 s_3 (\dot{\theta}_1 + \dot{\theta}_2) \\ a_1 c_{23} \dot{\theta}_1 + a_2 c_3 (\dot{\theta}_1 + \dot{\theta}_2) + a_3 (\dot{\theta}_1 + \dot{\theta}_2 + \dot{\theta}_3) \\ 0 \end{bmatrix} \\
{}^Tw_T &= {}^3w_3
\end{aligned}
$$

To get the velocity of the finger joint origins and the fingertip in relation to the frame $\{0\}$ of the hand, we multiply the velocity v with the corresponding rotational transformation.

$$
\begin{aligned}
{}^0v_1 &= \begin{bmatrix} 0 \\ 0 \\ 0 \end{bmatrix} \\
{}^0v_2 &= {}^0_2R \cdot {}^2v_2 = \begin{pmatrix} c_{12} & -s_{12} & 0 \\ s_{12} & c_{12} & 0 \\ 0 & 0 & 1 \end{pmatrix} \cdot \begin{bmatrix} a_1 s_2 \dot{\theta}_1 \\ a_1 c_2 \dot{\theta}_1 \\ 0 \end{bmatrix} = \begin{bmatrix} -a_1 s_1 \dot{\theta}_1 \\ a_1 c_1 \dot{\theta}_1 \\ 0 \end{bmatrix} \\
{}^0v_3 &= {}^0_3R \cdot {}^3v_3 = \begin{pmatrix} c_{123} & -s_{123} & 0 \\ s_{123} & c_{123} & 0 \\ 0 & 0 & 1 \end{pmatrix} \cdot \begin{bmatrix} a_1 s_{23} \dot{\theta}_1 + a_2 s_3 (\dot{\theta}_1 + \dot{\theta}_2) \\ a_1 c_{23} \dot{\theta}_1 + a_2 c_3 (\dot{\theta}_1 + \dot{\theta}_2) \\ 0 \end{bmatrix}
\end{aligned}
$$

$$\theta_2 = \cos^{-1}\left(\frac{({}^F x_T - a_3\cos\gamma)^2 + ({}^F y_T - a_3\sin\gamma)^2 - a_1^2 - a_2^2}{2a_1a_2}\right)$$

and

$$\begin{aligned} a_2^2 &= a_1^2 + d^2 - 2a_1 d\cos(\beta - \theta_1) \\ \cos(\beta - \theta_1) &= \frac{a_1^2 + d^2 - a_2^2}{2a_1 d} \end{aligned}$$

gives a solution for θ_1:

$$\begin{aligned} \theta_1 &= \beta - \cos^{-1}\left(\frac{a_1^2 + d^2 - a_2^2}{2a_1 d}\right) \\ &= \tan^{-1}\left(\frac{y}{x}\right) - \cos^{-1}\left(\frac{a_1^2 + d^2 - a_2^2}{2a_1 d}\right) \\ &= \tan^{-1}\left(\frac{y}{x}\right) - \cos^{-1}\left(\frac{a_1^2 + ({}^F x_T - a_3\cos\gamma)^2 + ({}^F y_T - a_3\sin\gamma)^2 - a_2^2}{2a_1\sqrt{({}^F x_T - a_3\cos\gamma)^2 + ({}^F y_T - a_3\sin\gamma)^2}}\right) \end{aligned}$$

Finally we get for θ_3:

$$\theta_3 = \gamma - \theta_1(x_T, y_t, \gamma) - \theta_2(x_T, y_t, \gamma)$$

Now we can get the correct angles φ_i as needed for the controller:

$$\begin{aligned} \varphi_1 &= \theta_1 - \alpha \\ \varphi_2 &= \theta_2 \\ \varphi_3 &= \theta_3 + \alpha \end{aligned}$$

D Dynamics of hand

D.1 Velocities

The velocity propagation from link to link is described by the following two equations

$${}^{i+1}v_{i+1} = {}^{i+1}_{i}R({}^i v_i + {}^i w_i \times {}^i P_{i+1})$$

for the linear velocity, and

$${}^{i+1}w_{i+1} = {}^{i+1}_{i}R\,{}^i w_i + \dot{\theta}_{i+1}\,{}^{i+1}\hat{Z}_{i+1}$$

for the angular velocity.

Now we can calculate the velocities of the joint origins for the fingers:

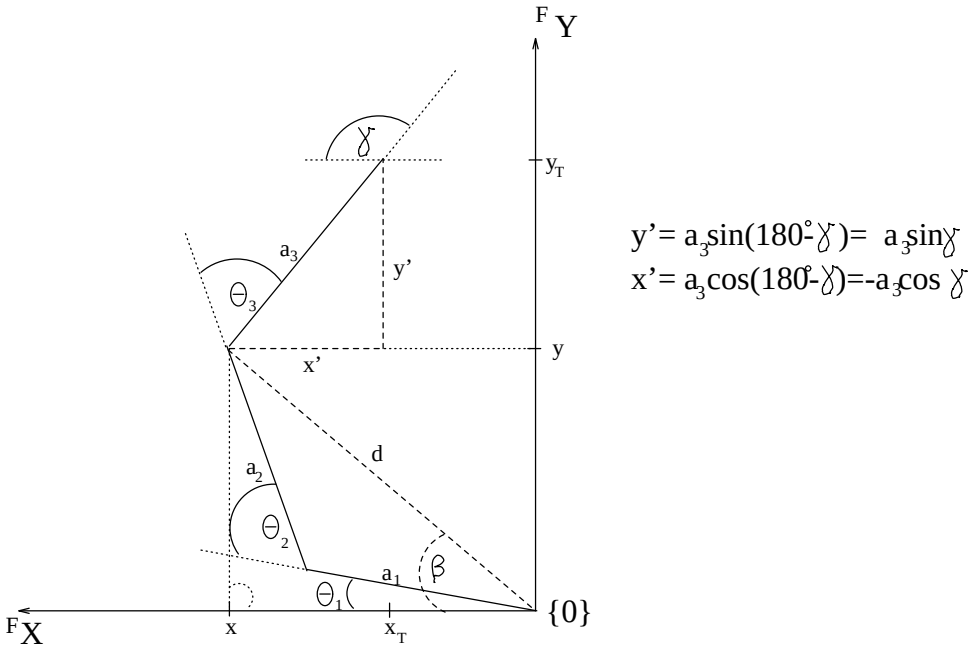

Figure 26: Inverse kinematics angle relations

the frame {P}. So we are looking for the coordinates $\theta_1(x_T, y_T, \gamma), \theta_2(x_T, y_T, \gamma)$, and $\theta_3(x_T, y_T, \gamma)$ expressed in terms of x_T, y_T, γ.

From Figure 26 one can easily see that $\gamma = \theta_1 + \theta_2 + \theta_3$. Since the angle γ is given, the origin of frame {3} is positioned at

$$\begin{aligned} x &= {}^F x_T + x' = {}^F x_T - a_3 \cos\gamma \\ y &= {}^F y_T - y' = {}^F y_T - a_3 \sin\gamma \end{aligned}$$

$$\text{where} \quad \begin{bmatrix} {}^F x_T \\ {}^F y_T \\ {}^F z_T \\ 1 \end{bmatrix} = {}^P_F T^{-1} \cdot \begin{bmatrix} {}^P x_T \\ {}^P y_T \\ {}^P z_T \\ 1 \end{bmatrix}$$

We get for the distance d:

$$d^2 = x^2 + y^2$$

Here we can make a solvability check by testing if $d \leq a_1 + a_2$.

By the law of cosine we get for the triangle $\triangle_{a_1 a_2 d}$:

$$d^2 = a_1^2 + a_2^2 - 2a_1 a_2 \cos(180° - \theta_2) = a_1^2 + a_2^2 + 2a_1 a_2 \cos\theta_2$$

which gives us a solution for θ_2:

$$\cos\theta_2 = \frac{d^2 - a_1^2 - a_2^2}{2a_1 a_2}$$

B.5 Fingertip to palm transformation

Now we are ready to derive the transformation that transforms vectors defined in the tool frame $\{T_j\}$ of the fingers to the palm frame {P} of the whole hand.

$$
\begin{aligned}
{}^{P}_{T_j}T &= {}^{P}_{F_j}T \cdot {}^{0}_{3}T_{F_j} \cdot {}^{3}_{T_j}T \qquad j = 2,3,4,5 \\
&= \begin{pmatrix} 1 & 0 & 0 & f_{jx} \\ 0 & 1 & 0 & f_{jy} \\ 0 & 0 & 1 & f_{jz} \\ 0 & 0 & 0 & 1 \end{pmatrix} \cdot \begin{pmatrix} c_{123} & -s_{123} & 0 & a_2c_{12} + a_1c_1 \\ s_{123} & c_{123} & 0 & a_2s_{12} + a_1s_1 \\ 0 & 0 & 1 & 0 \\ 0 & 0 & 0 & 1 \end{pmatrix} \cdot \begin{pmatrix} 1 & 0 & 0 & a_3 \\ 0 & 1 & 0 & 0 \\ 0 & 0 & 1 & 0 \\ 0 & 0 & 0 & 1 \end{pmatrix} \\
&= \begin{pmatrix} c_{123} & -s_{123} & 0 & a_3c_{123} + a_2c_{12} + a_1c_1 + f_{jx} \\ s_{123} & c_{123} & 0 & a_3s_{123} + a_2s_{12} + a_1s_1 + f_{jy} \\ 0 & 0 & 1 & f_{jz} \\ 0 & 0 & 0 & 1 \end{pmatrix}
\end{aligned}
$$

B.6 Thumb tip to palm transformation

To transform the tool frame of the thumb $\{T_1\}$ to the base frame of the palm {P} we have to use the transformation ${}^{P}_{F_1}T$ because the thumb is rotated 180° about the palm's Y axis.

$$
\begin{aligned}
{}^{P}_{T_1}T &= {}^{P}_{F_1}T \cdot {}^{0}_{3}T_{F_1} \cdot {}^{3}_{T_1}T \\
&= \begin{pmatrix} -1 & 0 & 0 & f_{jx} \\ 0 & 1 & 0 & f_{jy} \\ 0 & 0 & -1 & f_{jz} \\ 0 & 0 & 0 & 1 \end{pmatrix} \cdot \begin{pmatrix} c_{123} & -s_{123} & 0 & a_2c_{12} + a_1c_1 \\ s_{123} & c_{123} & 0 & a_2s_{12} + a_1s_1 \\ 0 & 0 & 1 & 0 \\ 0 & 0 & 0 & 1 \end{pmatrix} \cdot \begin{pmatrix} 1 & 0 & 0 & a_3 \\ 0 & 1 & 0 & 0 \\ 0 & 0 & 1 & 0 \\ 0 & 0 & 0 & 1 \end{pmatrix} \\
&= \begin{pmatrix} -c_{123} & s_{123} & 0 & -a_3c_{123} - a_2c_{12} - a_1c_1 + f_{jx} \\ s_{123} & c_{123} & 0 & a_3s_{123} + a_2s_{12} + a_1s_1 + f_{jy} \\ 0 & 0 & -1 & f_{jz} \\ 0 & 0 & 0 & 1 \end{pmatrix}
\end{aligned}
$$

C Inverse kinematics

Inverse kinematics is the problem of calculating the joint angles φ_i for the finger, given the desired position and orientation of the fingertip. Each finger of the hand is basically a three link miniature planar manipulator. It has 3 degrees of freedom: one for the angle of the fingertip and two for the position of the fingertip in the plane spanned by the finger. Let γ denote the angle between the X axis of the fingertip and the X axis of the palm, and let ${}^{P}x_T, {}^{P}y_T$ denote the position of the fingertip in

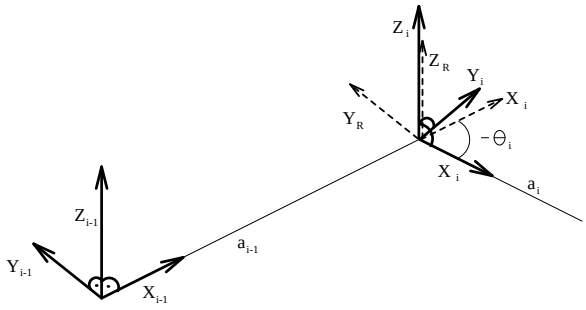

Figure 25: Finger link transformation

$$ {}^{R}_{i}T_{F_j} \;=\; R_Z(\theta_i) = \begin{pmatrix} \cos\theta_i & -\sin\theta_i & 0 & 0 \\ \sin\theta_i & \cos\theta_i & 0 & 0 \\ 0 & 0 & 1 & 0 \\ 0 & 0 & 0 & 1 \end{pmatrix} $$

So we get for the transformation from one joint to the next:

$$ {}^{i-1}_{i}T_{F_j} = {}^{i-1}_{R}T_{F_j} \cdot {}^{R}_{i}T_{F_j} = \begin{pmatrix} \cos\theta_i & -\sin\theta_i & 0 & a_{i-1} \\ \sin\theta_i & \cos\theta_i & 0 & 0 \\ 0 & 0 & 1 & 0 \\ 0 & 0 & 0 & 1 \end{pmatrix} $$

B.4 Finger transformations

Since we now have all the link transformations we can derive the transformation that relates frame {3} the final frame of the finger to its base frame {0}.

We will be using the conventions that $c_{123} = \cos(\theta_1 + \theta_2 + \theta_3)$ and $s_{123} = \sin(\theta_1 + \theta_2 + \theta_3)$; up to two angle identifiers may be omitted.

$$ \begin{aligned} {}^{0}_{3}T_{F_j} &= {}^{0}_{1}T_{F_j} \cdot {}^{1}_{2}T_{F_j} \cdot {}^{2}_{3}T_{F_j} \qquad j = 2,3,4,5 \\ &= \begin{pmatrix} c_1 & -s_1 & 0 & 0 \\ s_1 & c_1 & 0 & 0 \\ 0 & 0 & 1 & 0 \\ 0 & 0 & 0 & 1 \end{pmatrix} \cdot \begin{pmatrix} c_2 & -s_2 & 0 & a_1 \\ s_2 & c_2 & 0 & 0 \\ 0 & 0 & 1 & 0 \\ 0 & 0 & 0 & 1 \end{pmatrix} \cdot \begin{pmatrix} c_3 & -s_3 & 0 & a_2 \\ s_3 & c_3 & 0 & 0 \\ 0 & 0 & 1 & 0 \\ 0 & 0 & 0 & 1 \end{pmatrix} \\ &= \begin{pmatrix} c_{123} & -s_{123} & 0 & a_2c_{12} + a_1c_1 \\ s_{123} & c_{123} & 0 & a_2s_{12} + a_1s_1 \\ 0 & 0 & 1 & 0 \\ 0 & 0 & 0 & 1 \end{pmatrix} \end{aligned} $$

The transformations from the palm base to the finger base frames are given as follows:

$$ {}^{P}_{F_j}T = D_{F_j}(f_j) = \begin{pmatrix} 1 & 0 & 0 & f_{jx} \\ 0 & 1 & 0 & f_{jy} \\ 0 & 0 & 1 & f_{jz} \\ 0 & 0 & 0 & 1 \end{pmatrix} \qquad \text{where} \qquad j = 2,3,4,5. $$

The transformations from the palm base to the thumb is given by:

$$ {}^{P}_{F_1}T = D_{F_1}(f_1) \cdot R_Y(-180°) = \begin{pmatrix} -1 & 0 & 0 & f_{1x} \\ 0 & 1 & 0 & f_{1y} \\ 0 & 0 & -1 & f_{1z} \\ 0 & 0 & 0 & 1 \end{pmatrix} $$

with

$$ f = \begin{pmatrix} -3.0 & 14.5 & 14.5 & 14.5 & 14.5 \\ 1.8 & 0.4 & 0.4 & 0.4 & 0.4 \\ 5.0 & 7.5 & 2.5 & -2.5 & -7.5 \end{pmatrix} cm $$

B.3 Finger link transformation

In order to derive the transformation matrixes needed for forward kinematics we will first be deriving the transformation matrixes for each finger link. To simplify the analysis we define one intermediate frame $\{R_i\}$ for each link i. Let $\{R_i\}$ be the frame that we get by translating $\{P_{i-1}\}$ by the link length a_{i-1}. Frame $\{P_i\}$ now differs from the intermediate frame $\{R_i\}$ by a rotation θ_i with

$$ \begin{aligned} \theta_1 &= \varphi_1 + \alpha \\ \theta_2 &= \varphi_2 \\ \theta_3 &= \varphi_3 - \alpha \\ \text{with} \quad \alpha &= \frac{\pi}{4} - \tan^{-1}\left(\frac{4}{4.5}\right) \approx 0.0588 \approx 3.37° \end{aligned} $$

where φ_i describes the joint angles $0 \leq \varphi_i \leq 90°$ with i = 1,2,3.

Thus the transformation which transforms vectors defined in the frame $\{^iP\}$ to their description in $\{^{i-1}P\}$ is given by:

$$ \begin{aligned} {}^{i-1}P &= {}^{i-1}_{R}T_{F_j} \cdot {}^{R}_{i}T_{F_j} \cdot {}^{i}P \qquad j = 2,3,4,5 \\ \text{or} \quad {}^{i-1}P &= {}^{i-1}_{i}T_{F_j} \cdot {}^{i}P. \end{aligned} $$

Where we have the following for the intermediate transformations:

$$ {}^{i-1}_{R}T_{F_j} = D_X(a_{i-1}) = \begin{pmatrix} 1 & 0 & 0 & a_{i-1} \\ 0 & 1 & 0 & 0 \\ 0 & 0 & 1 & 0 \\ 0 & 0 & 0 & 1 \end{pmatrix} $$

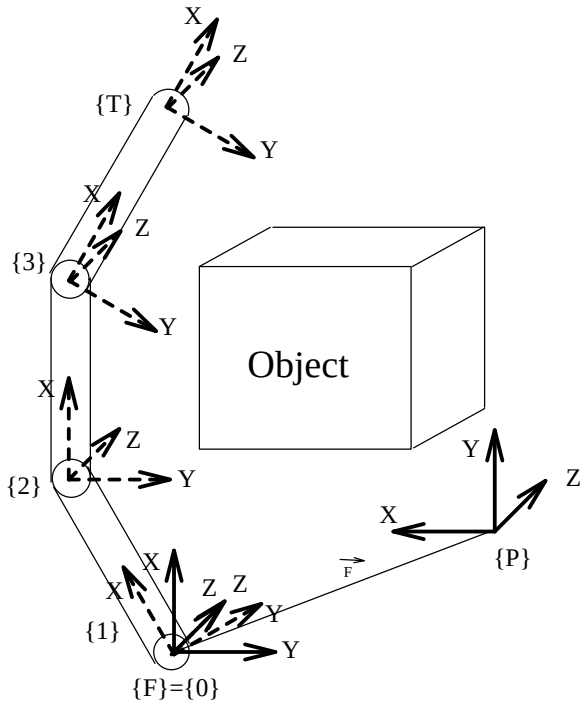

Figure 23: Frame definitions

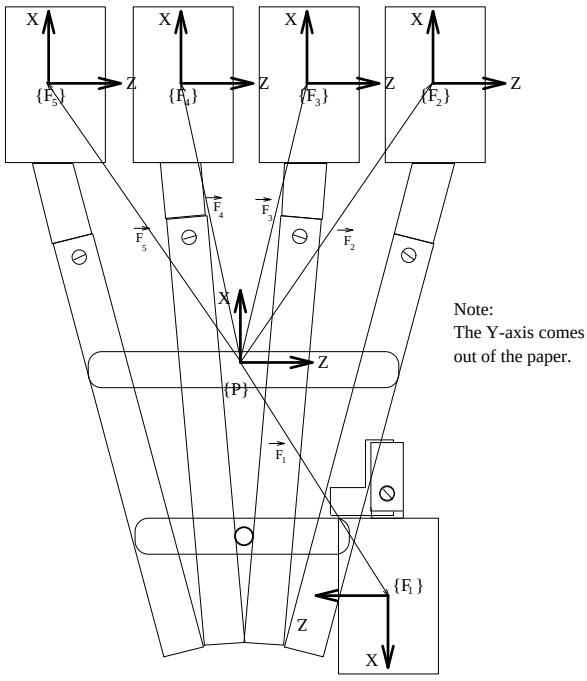

Figure 24: Palm frame definitions

B.1 Link parameters

We describe our direct drive hand in terms of the Denavit-Hartenberg notation and follow the link parameter description of Craig [3]:

a_i distance from $\hat{Z}_i$ to $\hat{Z}_{i+1}$ measured along $\hat{X}_i$
α_i angle between $\hat{Z}_i$ and $\hat{Z}_{i+1}$ measured about $\hat{X}_i$
d_i distance from $\hat{X}_{i-1}$ to $\hat{X}_i$ measured along $\hat{Z}_i$
θ_i angle between $\hat{X}_{i-1}$ and $\hat{X}_i$ measured about $\hat{Z}_i$

where $\hat{Z}_i$ is the unit vector that points along the joint axis i, $\hat{X}_i$ is the unit vector that points along the perpendicular between $\hat{Z}_i$ and $\hat{Z}_{i+1}$ from link i to link i+1. Finally $\hat{Y}_i$ is assigned according to the right hand rule.

Link parameters for one finger:

i	α_{i-1}	a_{i-1}	d_i	θ_i
1	0	0	0	θ_1
2	0	6.0cm	0	θ_2
3	0	6.0cm	0	θ_3
4	0	5.5cm	0	0

B.2 Frame definitions

For the calculations we use the following convention for naming the frames:

- **The finger base frame {F}**

  Each $\{F_j\}$ is located at the position on the palm where the knuckles are. {F} is stationary at all times.

- **Frames {0} through {3}**

  The finger link frames are numbered {0} to {3}. The frame {0} is identical to the finger base frame {F}. {3} is the frame of the last link.

- **The finger tool frame {T}**

  The frame {T} is affixed to the tip of the finger. It's transformation from the finger link frame {3} is given by

$$ {}^3_T T = D_X(a_3) = \begin{pmatrix} 1 & 0 & 0 & a_3 \\ 0 & 1 & 0 & 0 \\ 0 & 0 & 1 & 0 \\ 0 & 0 & 0 & 1 \end{pmatrix} $$

- **The palm base frame {P}**

  The frame {P} is affixed to the palm as shown in Figure 24.

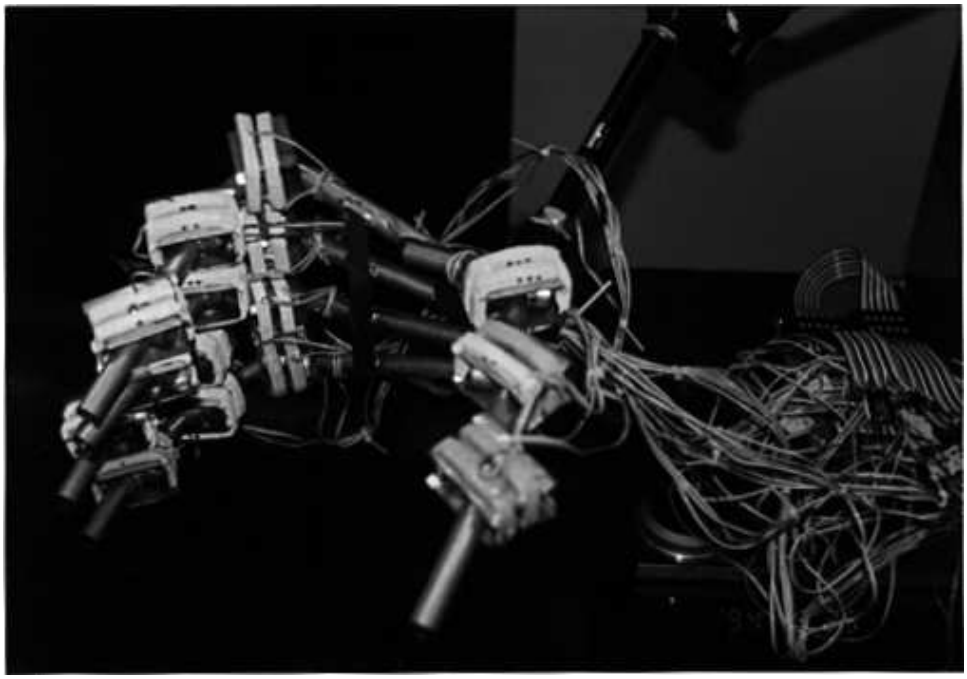

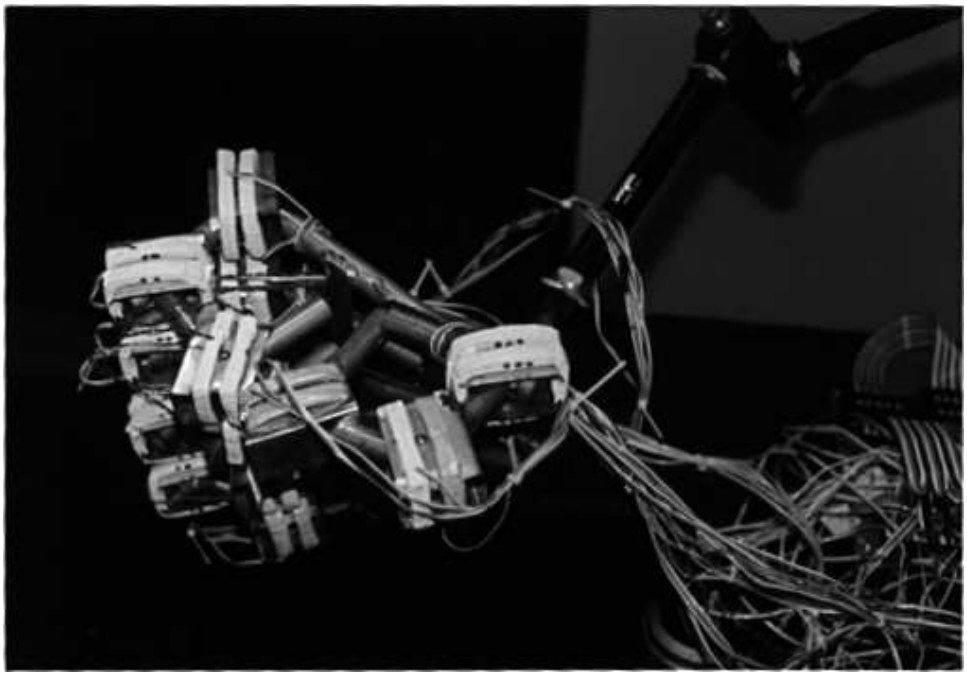

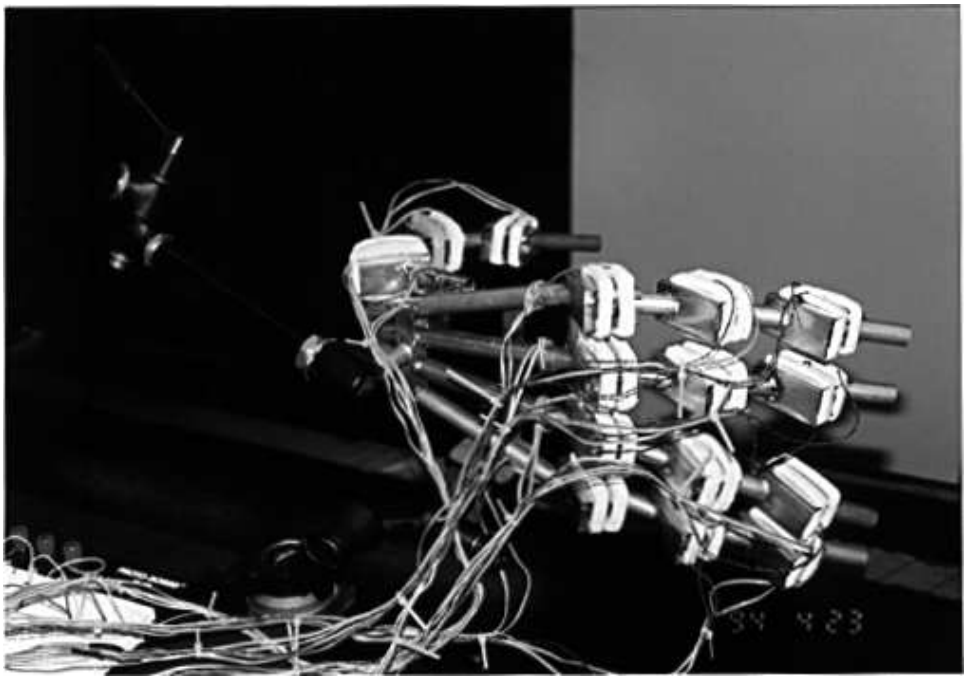

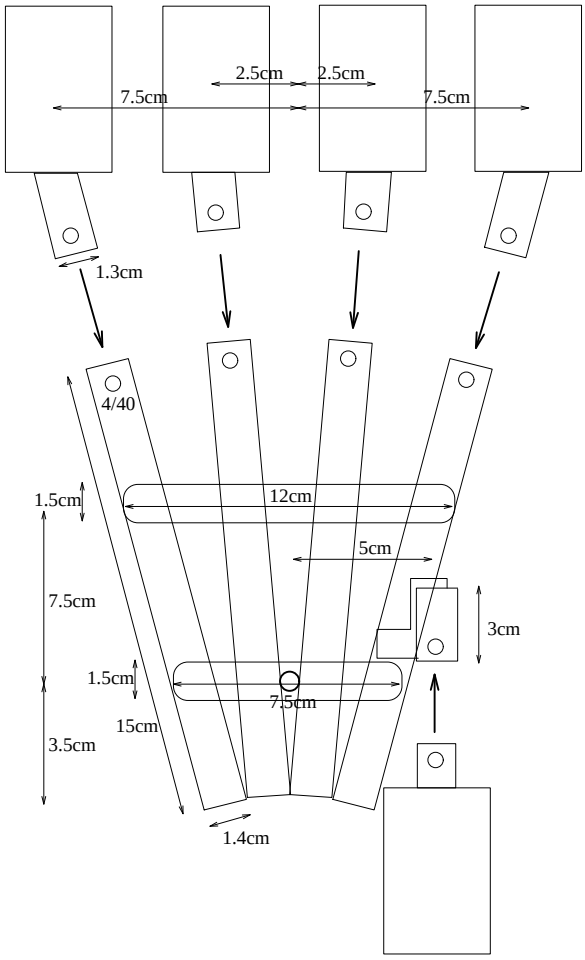

Figure 21: Hand assembly

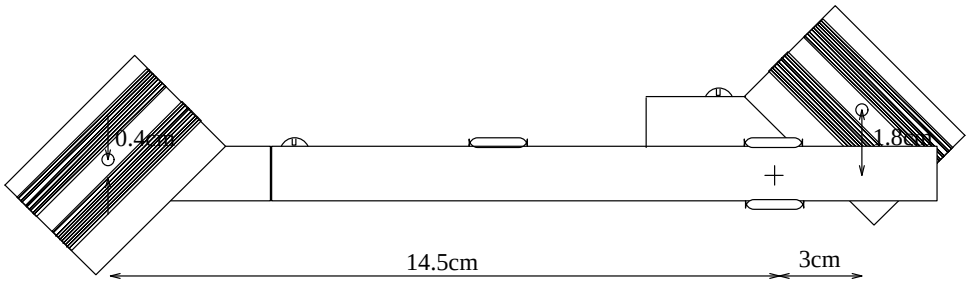

Figure 22: Side view of palm

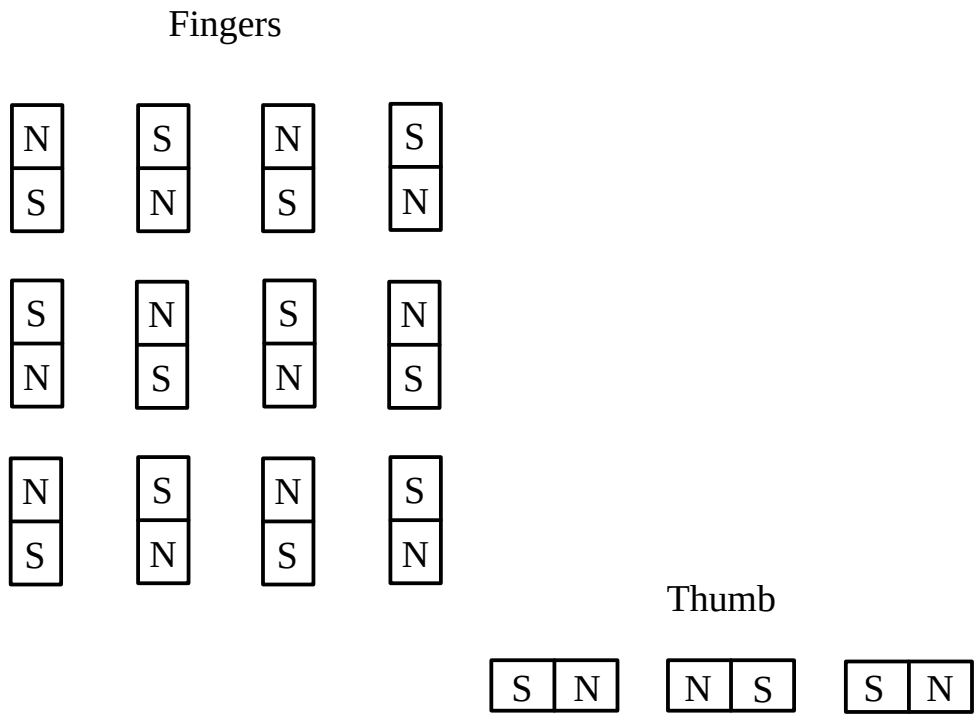

Figure 19: Magnet distribution

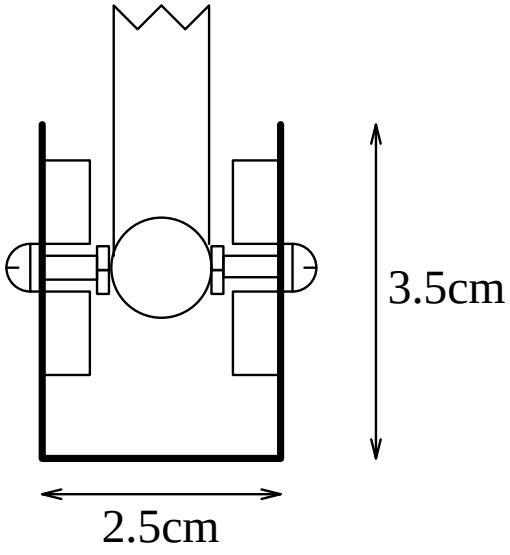

Figure 20: Side view of link

Magnets of Link 3:
Weight 0.195N

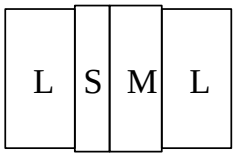

Magnets of Link 2:
Weight 0.265N

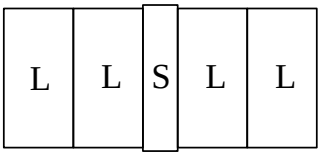

Magnets of Link 1:
Weight 0.325N

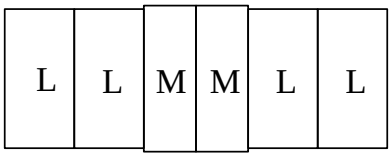

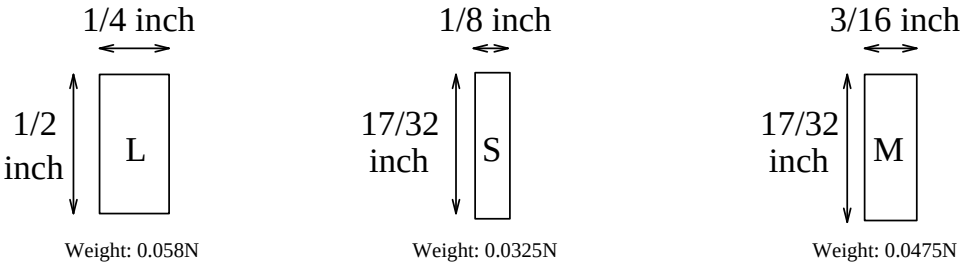

Total number of Magnets:

Small:	10	~ $3.00 each
Medium:	15	~ $3.50 each
Large:	60	~ $4.00 each
Total:		~ $292.50

Figure 18: Magnet sizes

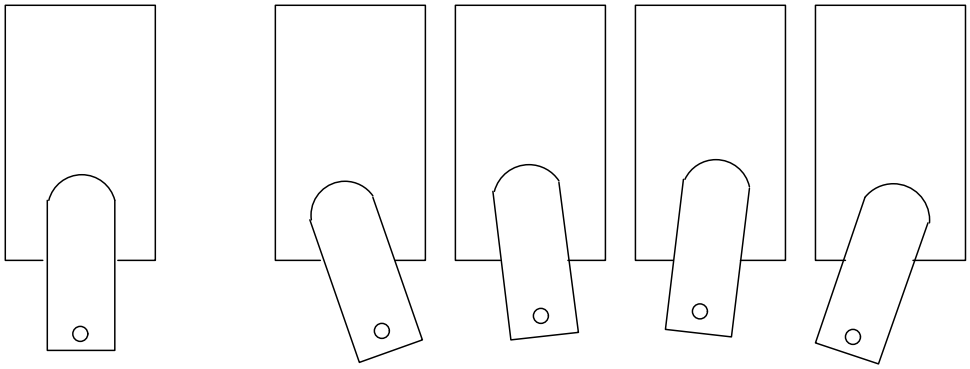

Figure 17: Finger to palm connectors

for the coils as well as a method to fasten the connection wires onto the coils. We encountered many problems due to wire shortings or wire ripping during use of the hand. The electrical tape seems to be the solution that worked the best.

After all the parts are completed, the magnets can be inserted according to the magnet distribution of Figure 19 and sizes according to Figure 18 into the magnet tubes. Next the coils can be put onto the bases. Then the links can be connected as shown in Figure 20.

A.2 Palm and hand construction

The palm is made out of 4 long brass tubes that resemble the bone structure of the human hand. Three pieces of brass plates were used to hold the brass tubes in position. These plates are soldered onto the tubes which gives quite a strong construction. We drilled a hole through the two brass plates closest to the wrist so that the hand may be fastened onto a conventional robot wrist. The fingers were placed on the palm as shown in Figure 21. Each finger is fastened onto the palm by inserting link 1 into the palm and fastening it with a screw. The side view of the palm is shown in Figure 22.

Initialy it was planned to mount the thumb at an angle of 90° on the palm. Unfortunately the fingers turned out to weigh more than what was expected. Since the torque at the fingers is not sufficient (within a reasonable power requirement) to lift the fingers into a horizontal position if the inside of the palm is showing downward, the thumb had to be mounted coplanar to the other fingers.

B Forward kinematics

One of the problems in the operation of a mechanical manipulator is how to calculate the position of the end effector if one knows the orientation of all links. This problem is known as forward kinematics.

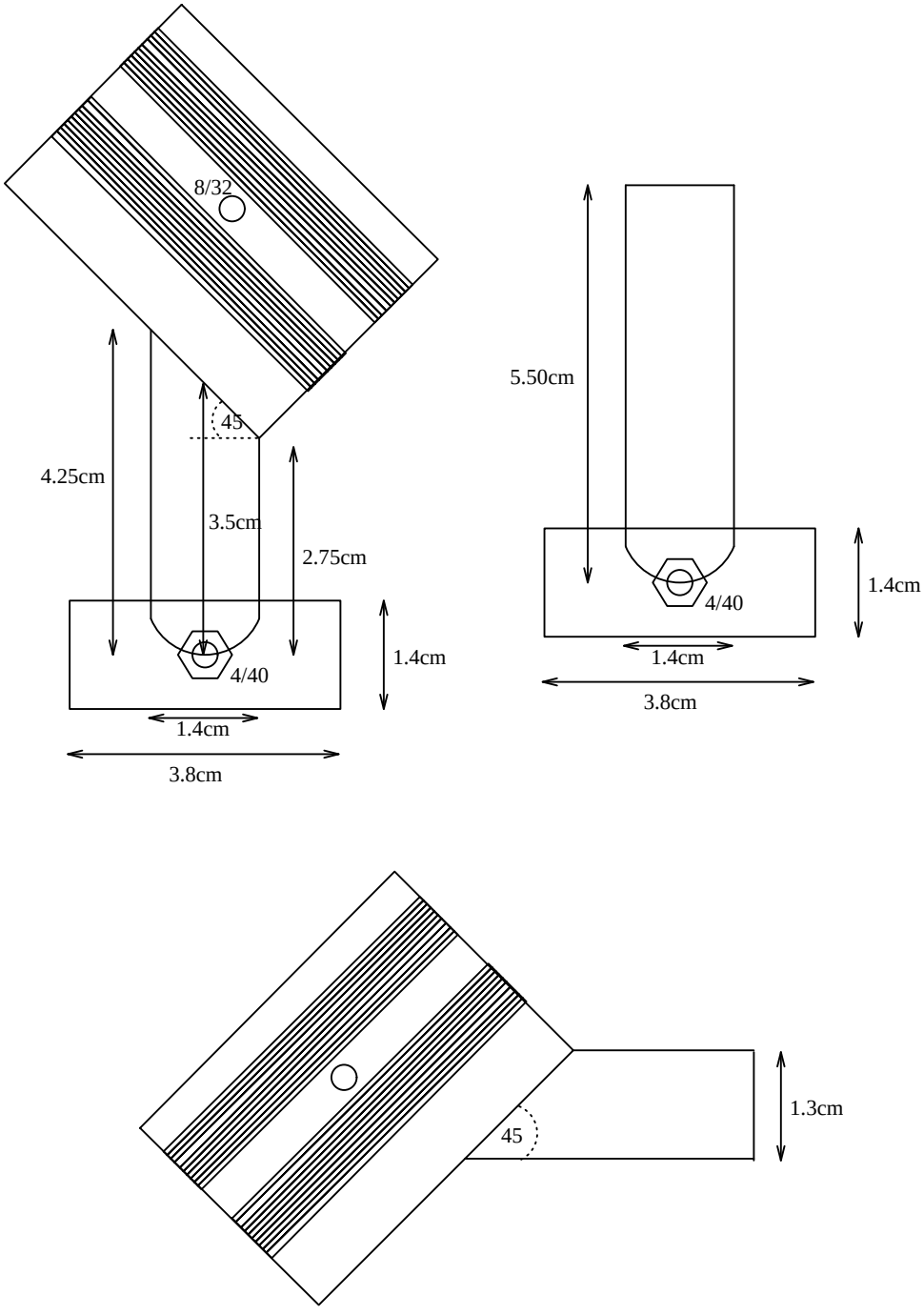

Figure 16: Finger link, finger tip and connection part to palm

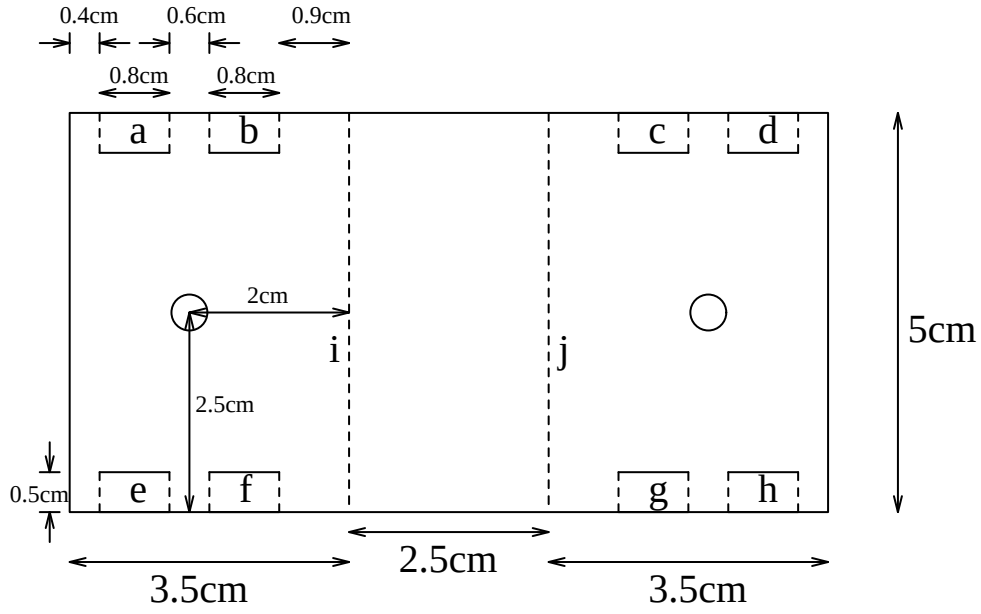

Figure 15: Base plate

workspace in each link. The base derives its size so that it can embody the magnet tube as well as the connection tube with a 90° workspace.

A.1 Finger construction

The bases are constructed out of a 0.01 inch thick brass plate. A simple metal scissors can be used to cut out the required size. Once the brass plate has the correct size, we cut a total of 16 incisions each of 5mm length along the side of the plate as shown in Figure 15. Next we bend the plate at positions a,b,d,e,f,g,h,i downwards. Once this is accomplished we bend the brass plate along the lines j and k also downwards. After the 8/32 holes are drilled into the base, its construction is complete.

For the bone-like structure we use brass tubes. These tubes are cut into the appropriate length as shown in Figure 16 .Next we grind a tube shaped hole into the end of the connection tube. The connection tube and the magnet tube are then soldered together. As a next step we drill a 4/40 hole into the magnet tube at the point where the axis is going to be. On both sides we then solder brass nuts. After this is done we grind down the 45° angle on the connection tube. Finally we solder the base and the connection tube together as shown in Figure 16. The finger tip is constructed in the same way as an ordinary connection tube and magnet tube. The only difference is that it is slightly longer.

For the fabrication of the coils we used a drilling machine with a custom form for the coils. We used a drilling speed of 380RPM and wound different sized coils for links 1,2 and 3 for 2min, 1.5min and 1min respectively. After the coils were completed we wrapped them in electrical tape that can withstand 105°C. This provides isolation

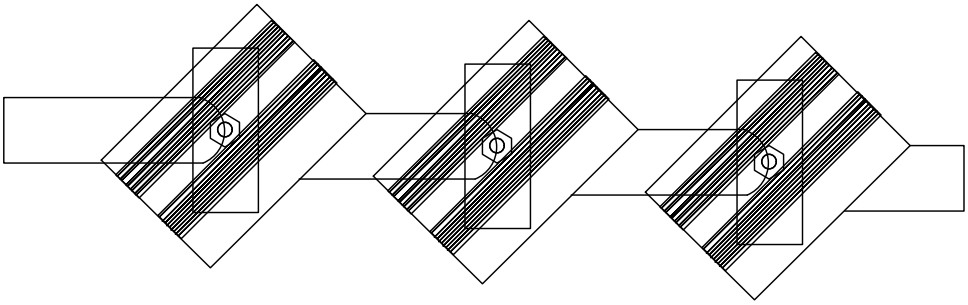

Figure 13: Fully extended finger

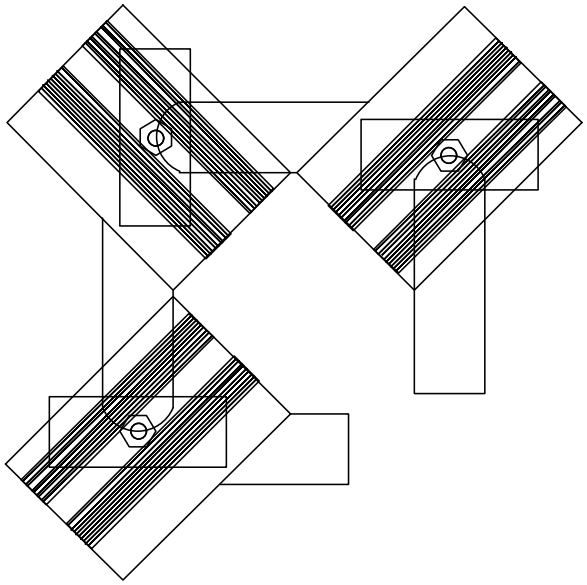

Figure 14: Finger completely collapsed

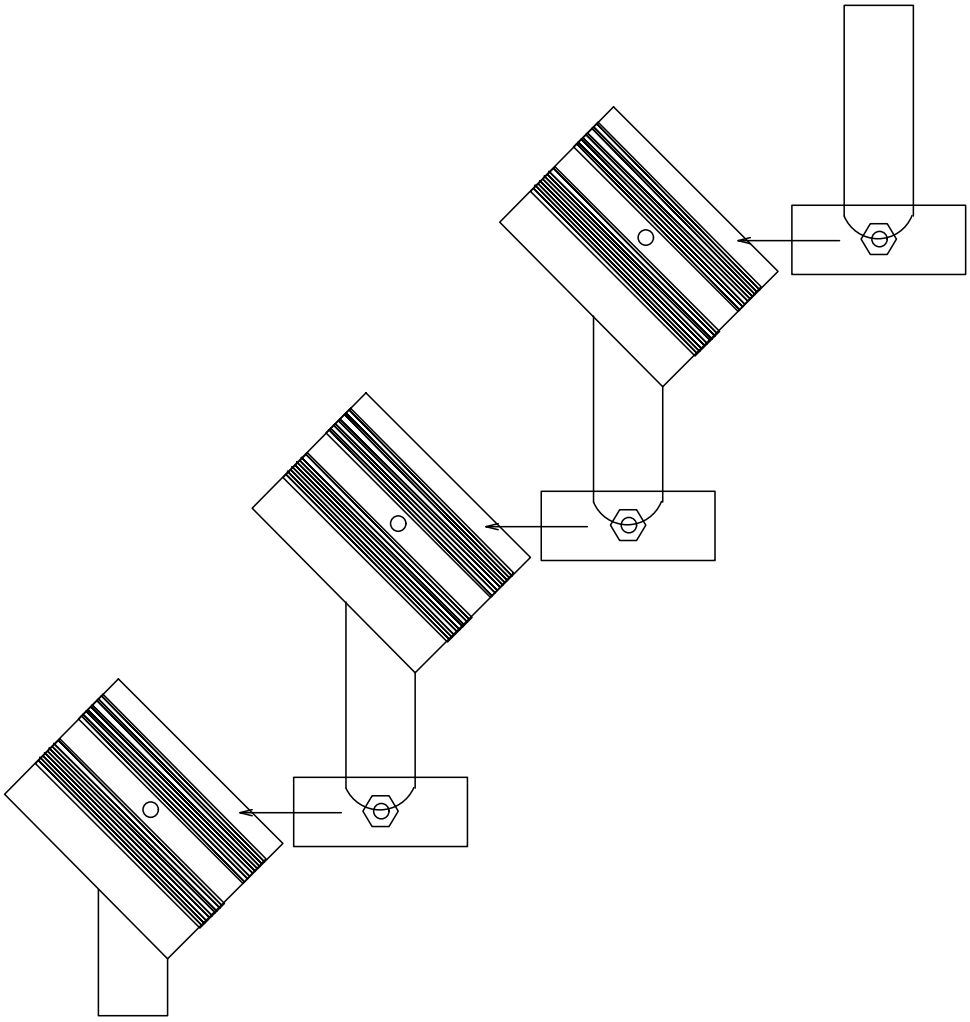

Figure 12: 4 parts constitute a finger

A Construction of hand

One finger consists of 4 parts (Figure 12):

- Base with connection to palm,
- two links,
- and the finger tip.

A fully extended finger is shown in Figure 13. One finger completely bent inwards (as in a fist) is shown in Figure 14. The thumb is identical to the other fingers.

The size of the individual fingers and the final hand is due to the size of the magnets that are embedded inside the magnet tubes. These magnets have a diameter of exactly 1/2 inch. Since our goal was to construct a human-like hand we had to achieve a 90°

theoretical and experimentally. Also a graphics interface has been developed for the hand.

The construction of the hand has given valuable insights to the development of a more precise and human sized direct drive hand. Another even smaller sized prototype finger has been built by Prof. Richard Wallace and Louis Arauz. Fred Hansen has begun to construct universal links that will be used for a precision direct drive hand. These links are highly symmetric about the X axis and can thus lead to more accurate modeling and control.

Using the kinematic calibration method by An et al. [10] one should compare how error levels in the kinematic and dynamic parameters scale from large robotics devices to miniature robotics devices. The comparison of computed torque control and feed forward control for miniature direct drive devices also needs to be made.

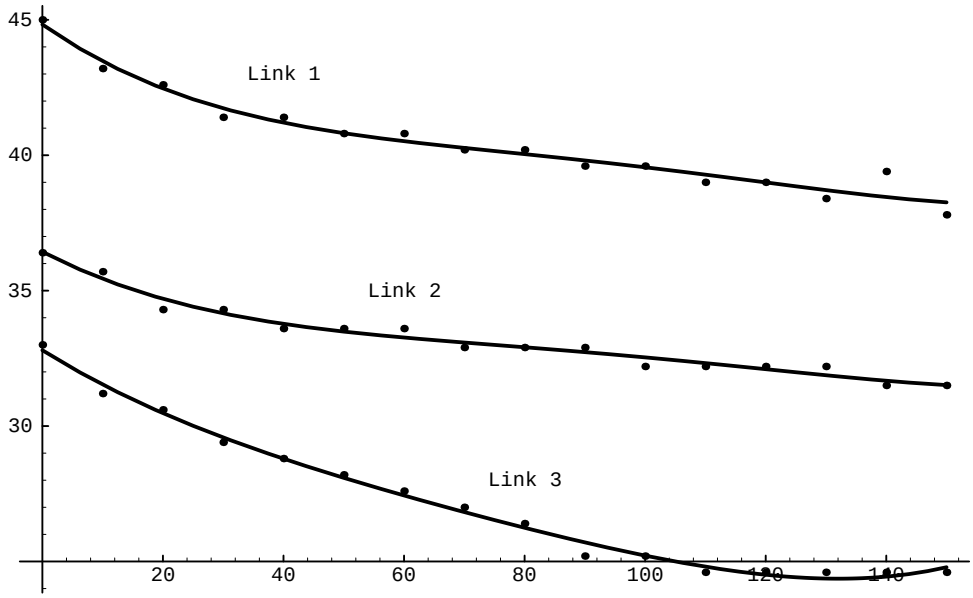

Figure 10: Torque over time for U=20V $\tau[10^{-3}Nm](t[s])$

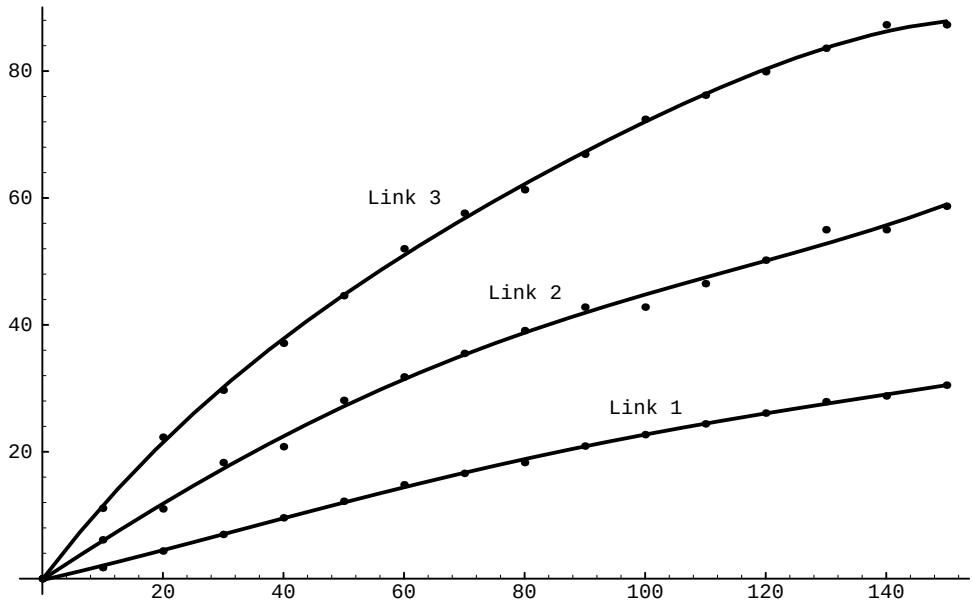

Figure 11: Temperature over time for U=20V $\Delta T[K](t[s])$

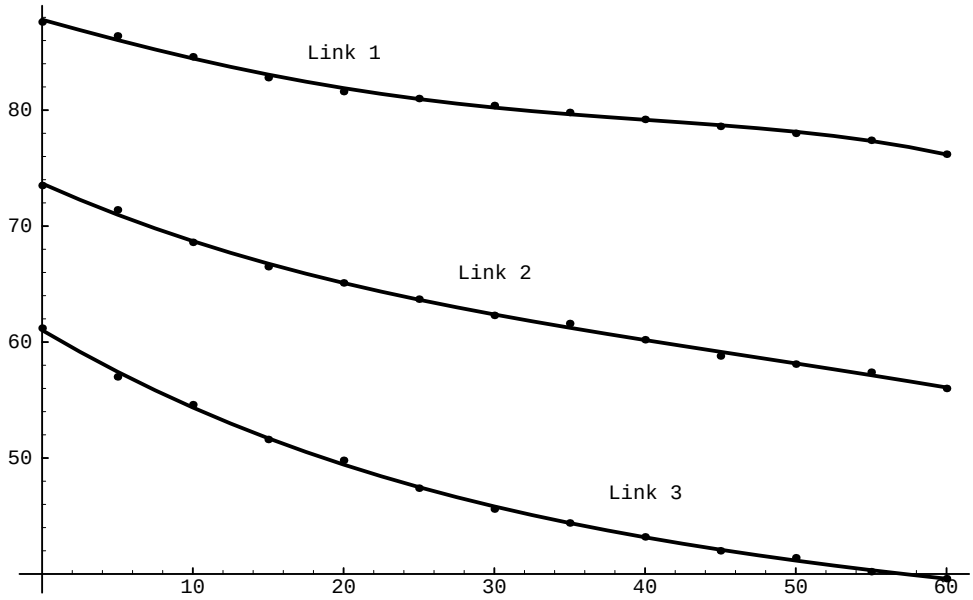

Figure 8: Torque over time for U=40V $\tau[10^{-3}Nm](t[s])$

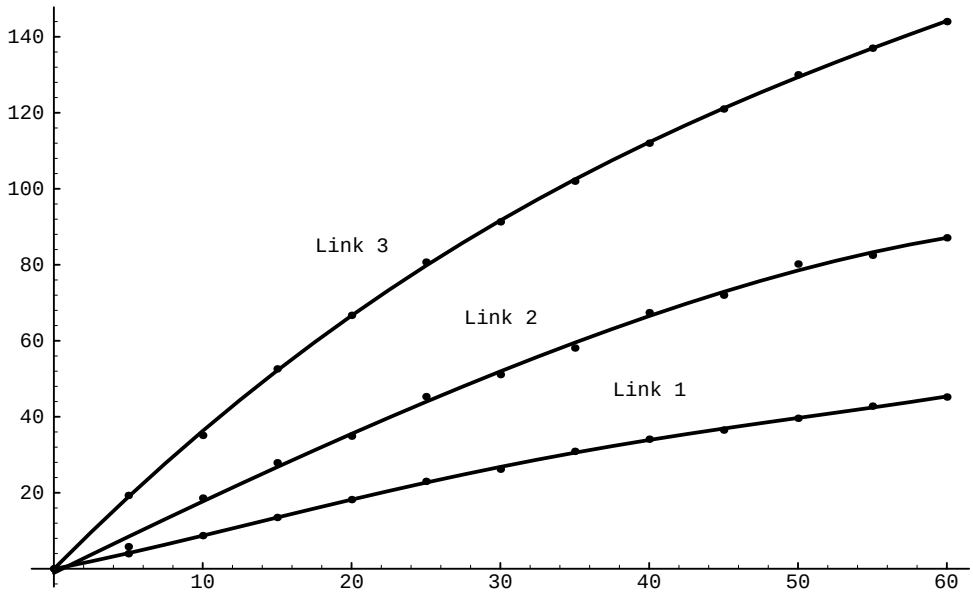

Figure 9: Temperature over time for U=40V $\Delta T[K](t[s])$

5.6 Changes in torque as coils heat up

$U_{sup} = 40V$

	Link 1 $U_{coil} = 38.2V$			Link 2 $U_{coil} = 37.4V$			Link 3 $U_{coil} = 36.3V$		
t (s)	I (A)	τ_{max} $(10^{-3}Nm)$	$\Delta T^*)$ (K)	I (A)	τ_{max} $(10^{-3}Nm)$	$\Delta T^*)$ (K)	I (A)	τ_{max} $(10^{-3}Nm)$	$\Delta T^*)$ (K)
0	1.18	87.6	0	1.71	73.5	0	2.50	61.2	0
5	1.17	86.4	3.96	1.67	71.4	5.81	2.32	57.0	19.3
10	1.15	84.6	8.72	1.59	68.6	18.6	2.20	54.6	35.1
15	1.13	82.8	13.5	1.54	66.5	27.9	2.08	51.6	52.6
20	1.11	81.6	18.2	1.50	65.1	34.9	1.98	49.8	66.7
25	1.09	81.0	23.0	1.45	63.7	45.3	1.90	47.4	80.7
30	1.08	80.4	26.2	1.42	62.3	51.1	1.84	45.6	91.3
35	1.06	79.8	30.9	1.39	61.6	58.1	1.79	44.4	102.0
40	1.05	79.2	34.1	1.35	60.2	67.4	1.74	43.2	112.0
45	1.04	78.6	36.5	1.33	58.8	72.0	1.70	42.0	121.0
50	1.03	78.0	39.6	1.30	58.1	80.2	1.66	41.4	130.0
55	1.02	77.4	42.8	1.29	57.4	82.5	1.63	40.2	137.0
60	1.01	76.2	45.2	1.27	56.0	87.1	1.60	39.6	144.0

$U_{sup} = 20V$

	Link 1 $U_{coil} = 19.0V$			Link 2 $U_{coil} = 18.7V$			Link 3 $U_{coil} = 18.0V$		
t (s)	I (A)	τ_{max} $(10^{-3}Nm)$	$\Delta T^*)$ (K)	I (A)	τ_{max} $(10^{-3}Nm)$	$\Delta T^*)$ (K)	I (A)	τ_{max} $(10^{-3}Nm)$	$\Delta T^*)$ (K)
0	0.651	45.0	0	0.90	36.4	0	1.31	33.0	0
10	0.646	43.2	1.74	0.88	35.7	6.12	1.26	31.2	11.1
20	0.640	42.6	4.36	0.86	34.3	11.0	1.21	30.6	22.3
30	0.633	41.4	6.97	0.84	34.3	18.3	1.18	29.4	29.7
40	0.627	41.4	9.59	0.83	33.6	20.8	1.15	28.8	37.1
50	0.621	40.8	12.2	0.81	33.6	28.1	1.12	28.2	44.6
60	0.615	40.8	14.8	0.80	33.6	31.8	1.09	27.6	52.0
70	0.611	40.2	16.6	0.79	32.9	35.5	1.07	27.0	57.6
80	0.607	40.2	18.3	0.78	32.9	39.1	1.06	26.4	61.3
90	0.602	39.6	20.9	0.77	32.9	42.8	1.04	25.2	66.9
100	0.598	39.6	22.7	0.77	32.2	42.8	1.02	25.2	72.4
110	0.594	39.0	24.4	0.76	32.2	46.5	1.01	24.6	76.2
120	0.590	39.0	26.1	0.75	32.2	50.2	1.00	24.6	79.9
130	0.587	38.4	27.9	0.74	32.2	55.0	0.99	24.6	83.6
140	0.584	38.4	28.8	0.74	31.5	55.0	0.98	24.6	87.3
150	0.581	37.8	30.5	0.73	31.5	58.7	0.98	24.6	87.3

*) calculated data according to $R = R_0(1 + \alpha\Delta T)$ with $\alpha = 0.00393\frac{1}{K}$

6 Conclusion and ongoing research

We have designed and built a direct drive hand that is only about twice the size of a human hand. The properties of the hand have been analyzed thoroughly both

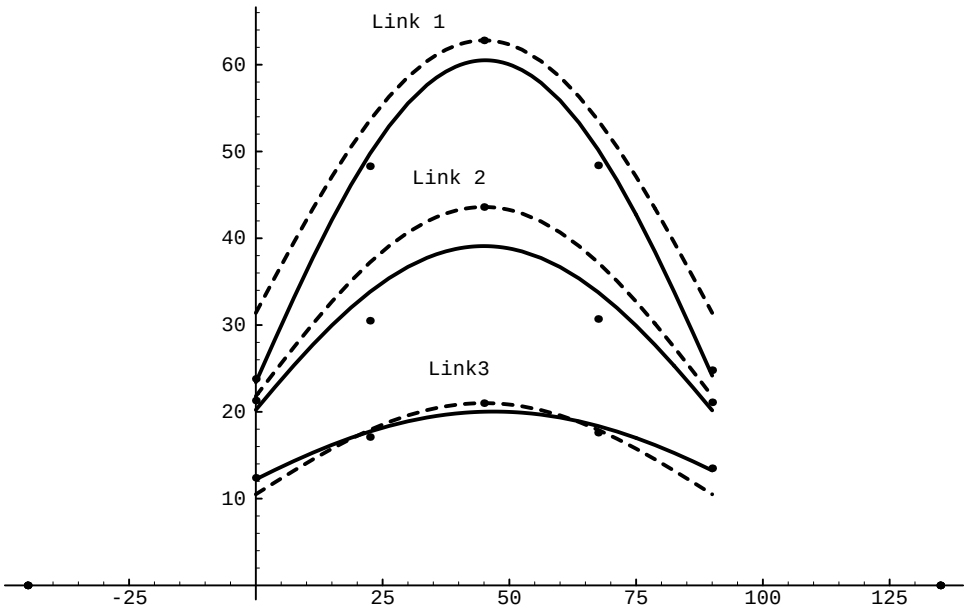

Figure 6: Torque constant $K_T[10^{-3}\frac{Nm}{A}](\theta[^\circ])$

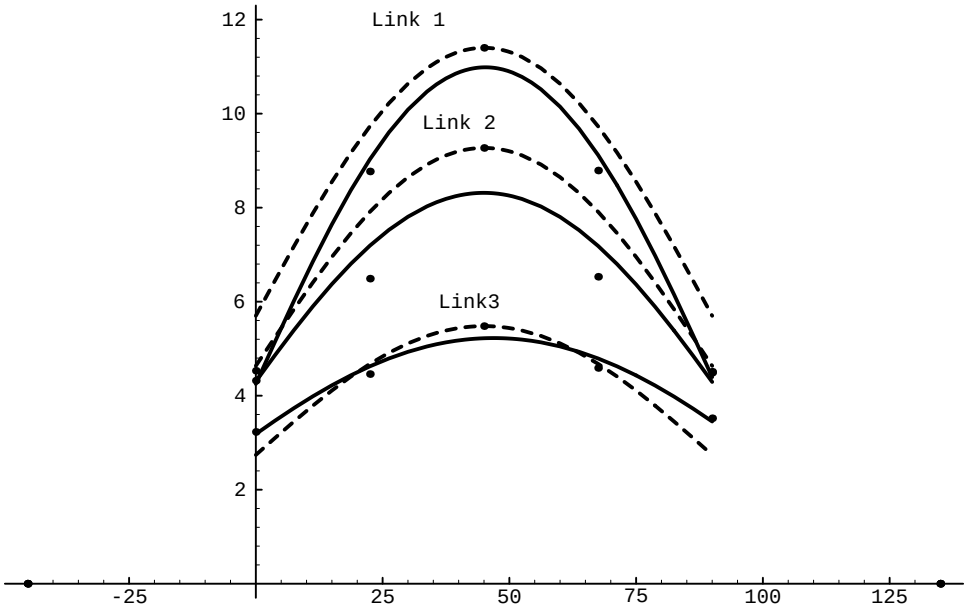

Figure 7: Motor constant $K_M[10^{-3}\frac{Nm}{\sqrt{W}}](\theta[^\circ])$

Link 2 Finger 1: $R = 22.1\Omega$

U(V)	I(A)	$\tau(10^{-3}Nm)$ $\varphi = 0°$	$\tau(10^{-3}Nm)$ $\varphi = 22.5°$	$\tau(10^{-3}Nm)$ $\varphi = 45°$	$\tau(10^{-3}Nm)$ $\varphi = 67.5°$	$\tau(10^{-3}Nm)$ $\varphi = 90°$
2.5	0.11	0	2.1	4.9	2.8	0
5.0	0.23	2.8	4.9	9.1	6.3	3.5
7.5	0.34	5.6	9.8	12.6	10.5	6.3
10.0	0.45	9.1	13.3	18.2	14.7	9.1
12.5	0.57	11.2	17.5	23.8	18.9	11.2
15.0	0.68	14.7	21.7	28.7	22.4	14.7
17.5	0.79	16.8	25.9	33.6	25.2	16.8
20.0	0.90	19.6	29.4	39.9	30.1	19.6
22.5	1.02	21.7	31.5	44.1	32.2	21.7
25.0	1.13	24.5	35.7	49.7	35.0	23.8
27.5	1.24	25.9	37.8	53.2	37.8	25.9
30.0	1.36	28.7	42.0	58.8	39.9	28.0
32.5	1.47	32.2	43.4	63.7	42.7	30.8
35.0	1.58	34.3	45.5	69.3	45.5	32.9
37.5	1.70	36.4	47.6	77.0	48.3	36.4
40.0	1.81	38.5	50.4	84.0	51.8	39.2
$K_T(10^{-3}\frac{Nm}{A})$		21.3	30.5	43.6	30.7	21.1
$K_M(10^{-3}\frac{Nm}{\sqrt{W}})$		4.53	6.49	9.27	6.53	4.49

Link 3 Finger 1: $R = 14.7\Omega$

U(V)	I(A)	$\tau(10^{-3}Nm)$ $\varphi = 0°$	$\tau(10^{-3}Nm)$ $\varphi = 22.5°$	$\tau(10^{-3}Nm)$ $\varphi = 45°$	$\tau(10^{-3}Nm)$ $\varphi = 67.5°$	$\tau(10^{-3}Nm)$ $\varphi = 90°$
2.5	0.17	2.8	4.2	4.9	4.9	4.2
5.0	0.34	4.9	7.7	9.1	8.4	7.0
7.5	0.51	7.7	11.2	13.3	11.2	9.1
10.0	0.68	10.5	12.6	17.5	14.0	11.2
12.5	0.85	12.6	15.4	21.0	16.8	12.6
15.0	1.02	14.7	17.5	24.5	17.5	14.7
17.5	1.19	16.8	21.0	28.0	22.4	16.1
20.0	1.36	18.2	23.1	31.5	25.2	17.5
22.5	1.53	18.9	25.9	33.6	28.0	19.6
25.0	1.70	20.3	29.4	33.6	30.8	21.7
27.5	1.87	21.7	32.2	35.7	32.9	23.8
30.0	2.04	22.4	35.7	38.5	34.3	25.9
32.5	2.21	23.8	36.4	42.0	35.7	28.7
35.0	2.38	25.9	38.5	45.5	39.2	31.5
37.5	2.55	28.7	42.7	48.3	42.0	35.7
40.0	2.72	32.2	45.5	53.2	45.5	39.9
$K_T(10^{-3}\frac{Nm}{A})$		12.4	17.1	21.0	17.6	13.5
$K_M(10^{-3}\frac{Nm}{\sqrt{W}})$		3.23	4.46	5.48	4.59	3.52

5.4 Static power requirement for U=40V

number of coils	coils size	I
10	small	14.17 A
10	medium	9.39 A
10	large	7.01 A
total		30.57 A

Total power requirement

$$P = U \cdot I = 40V \cdot 30.57A = 1.2kW$$

5.5 Torque

The double line in the tables indicates which torque values were used to calculate the torque constant. All values above the double line were disregarded.

In Figure 6 and Figure 7 the thick line denotes a 4^{th} order polynomial approximation of the points given and the dashed line describes the function $K_{Tmax} \cdot \sin^2(\theta + 45°)$ and $K_{Mmax} \cdot \sin^2(\theta + 45°)$ respectively.

Link 1 Finger 1: $R = 30.3\Omega$

U(V)	I(A)	$\tau(10^{-3}Nm)$ $\varphi = 0°$	$\tau(10^{-3}Nm)$ $\varphi = 22.5°$	$\tau(10^{-3}Nm)$ $\varphi = 45°$	$\tau(10^{-3}Nm)$ $\varphi = 67.5°$	$\tau(10^{-3}Nm)$ $\varphi = 90°$
2.5	0.08	0.0	0.0	0.0	0.0	0.0
5.0	0.17	0.0	0.0	0.0	0.0	0.0
7.5	0.25	0.0	8.4	11.2	11.9	0.0
10.0	0.33	2.8	11.9	16.1	16.8	3.5
12.5	0.41	4.9	18.9	24.5	21.0	4.9
15.0	0.50	7.7	21.7	32.9	25.2	8.4
17.5	0.58	11.2	25.2	36.4	29.4	10.5
20.0	0.66	13.3	29.4	39.2	33.6	12.6
22.5	0.74	15.4	35.0	48.3	37.8	15.4
25.0	0.83	18.2	38.5	53.2	39.9	19.6
27.5	0.91	21.0	44.1	56.0	41.3	22.4
30.0	0.99	23.8	47.6	60.9	45.5	26.6
32.5	1.07	27.3	53.2	65.8	49.7	29.4
35.0	1.16	30.8	58.8	71.4	54.6	33.2
37.4	1.23	34.3	63.7	79.1	60.2	35.7
40.0	1.32	37.8	70.0	86.8	65.1	39.2
$K_T(10^{-3}\frac{Nm}{A})$		23.8	48.3	62.8	48.4	24.8
$K_M(10^{-3}\frac{Nm}{\sqrt{W}})$		4.32	8.77	11.4	8.79	4.51

5.1 Weight of parts

Part	Weight (g)
Link 1 (complete)	104.0
Link 2 (complete)	80.0
Link 3 (complete)	32.0
Link 1 (brass only)	13.5
Link 2 (brass only)	13.5
Link 3 (brass only)	12.5
Link 1 (magnets)	32.5
Link 2 (magnets)	26.5
Link 3 (magnets)	19.5
Small magnet	3.25
Medium magnet	4.75
Large magnet	5.80
Small coil	20.0
Medium coil	29.0
Large coil	38.0

5.2 Resistance of coils

Joint	Finger	1	2	3	4	5
1	lower	57.4	56.9	57.4	57.7	57.5
	upper	57.0	<u>54.6</u>	57.7	57.3	57.2
2	lower	42.0	43.1	42.4	42.8	42.5
	upper	42.8	41.7	42.6	42.4	<u>43.8</u>
3	lower	28.0	28.7	29.3	<u>29.5</u>	27.5
	upper	27.6	28.4	27.5	28.4	27.4

The underlined entries are those that deviate the most from the average coil resistance for its class.

5.3 Average resistance of coils

coil size	winding time *)	R	$\overline{R}$	maximum error
large	$\approx 2.00min$	$\approx 60\Omega$	57.1Ω	4.33%
medium	$\approx 1.50min$	$\approx 45\Omega$	42.6Ω	2.79%
small	$\approx 1.00min$	$\approx 30\Omega$	28.2Ω	4.50%

*) Drill speed 380RPM

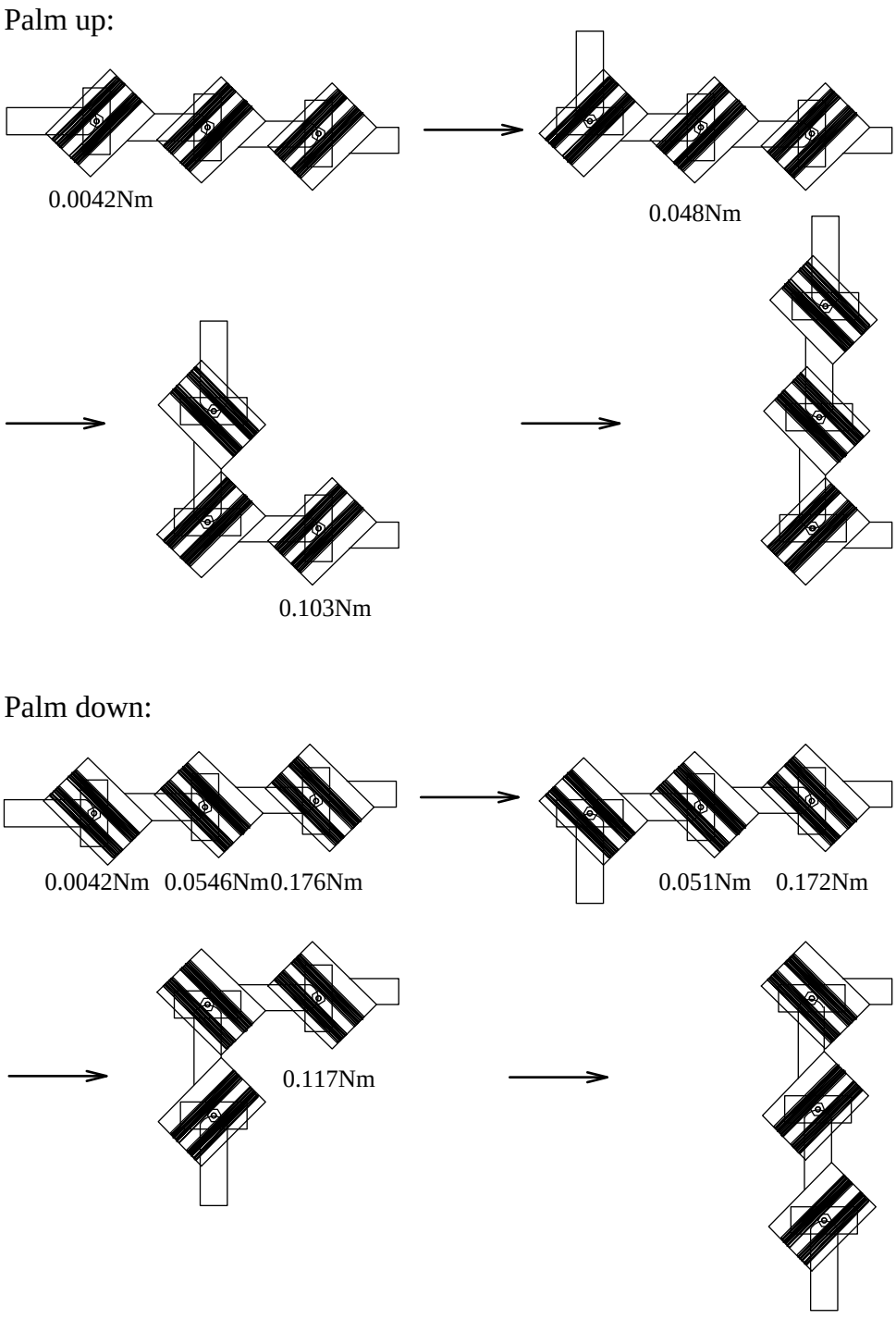

Figure 5: Measured torque requirements

5 Experiments

We conducted a number of experiments to measure the torque at each finger joint, the result of which can be found in the tables below. The measures were made with a Mark-10 force meter and a 12.5cm extension mounted onto the tip of the force meter. The torque measurements were done with great care in order to get the most accurate data possible. During the measurements the hand was mounted on a photo-arm and the joints other than the one measured were held in place by strings. However due to the large extension used and small inaccuracies in the hand every source of error could not be eliminated. This explains the divergence between the data for the torque and the torque/heat measurements for which the same care could not be applied in order not to destroy the coils.

The measured data tells us the power requirement to lift one finger into the horizontal position with the inside of the palm pointing downward. To bring the hand into this configuration requires torques of $4.2 \cdot 10^{-3}$Nm, $54.6 \cdot 10^{-3}$Nm and $176 \cdot 10^{-3}$Nm (measured data) for links 3, 2 and 1 respectively. This gives us a current requirement of 0.34A, 2.56A and 7.39A respectively which equals 9.0kW for the whole hand. To lift a finger with the palm pointed upward we need torques of $4.2 \cdot 10^{-3}$Nm, $48.1 \cdot 10^{-3}$Nm and $103 \cdot 10^{-3}$Nm (measured data) for link 3, 2 and 1 respectively. Which gives a current requirement of 0.34A, 2.26A and 4.33A respectively which equals 3.4kW for the whole hand. The torque requirements are illustrated in Figure 5.

Experimentally we confirmed that 0.33A and 2.1A are enough for the finger links 2 and 3 respectively to operate the hand at any angle. The amount of current needed for link 3 was not verified due to the high currents involved. Needless to say that the hand can only be operated with such a high current for short periods of time due to the coils heating up (see table below for heat limitations).

However dynamically we need much less power to lift the finger. Experiments showed that a power requirement of 3kW is sufficient to completely close a finger with the palm pointed upward. We showed this by applying 40V with a 15A maximum power supply to the coils of one finger.

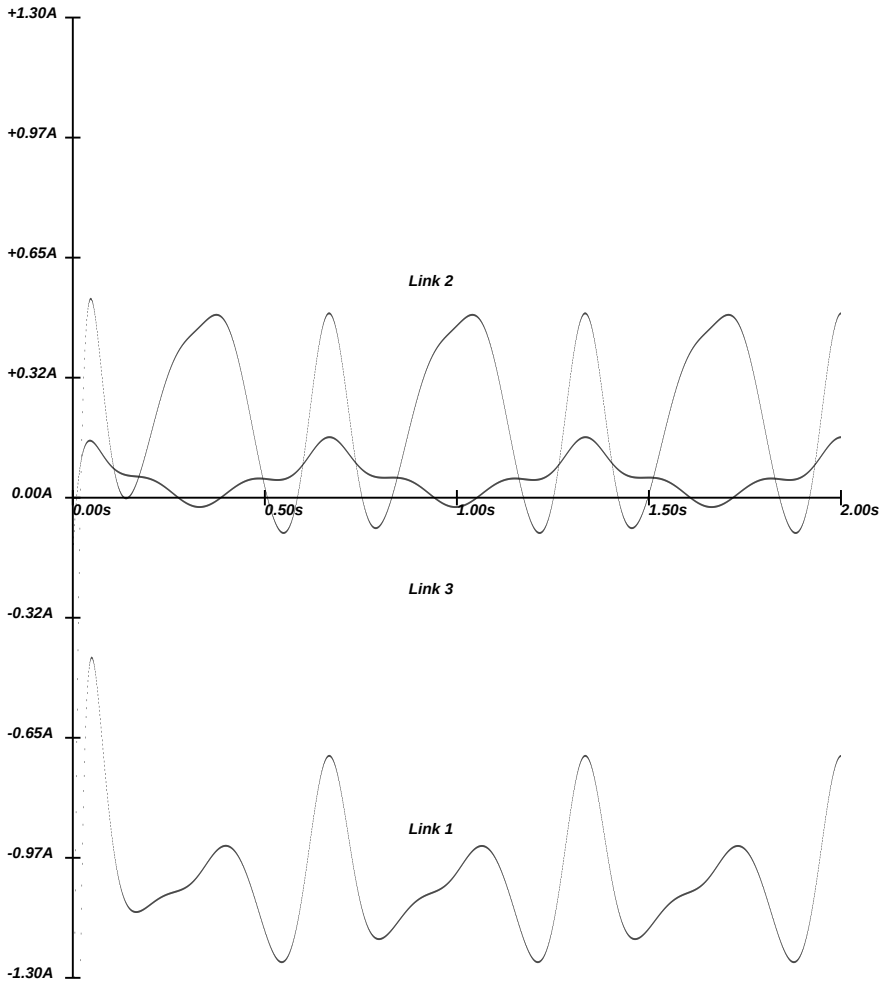

Figure 4: Current requirements to move a perfectly modeled finger from $\theta_i = 2.5°$ to $\theta_i = 87.5°$ and back three times in two seconds (gravity vector parallel to Y axis of palm) and an update frequency of 1kHz (100Hz would give the same result but the graph would not be as clear due to large steps in the plot)

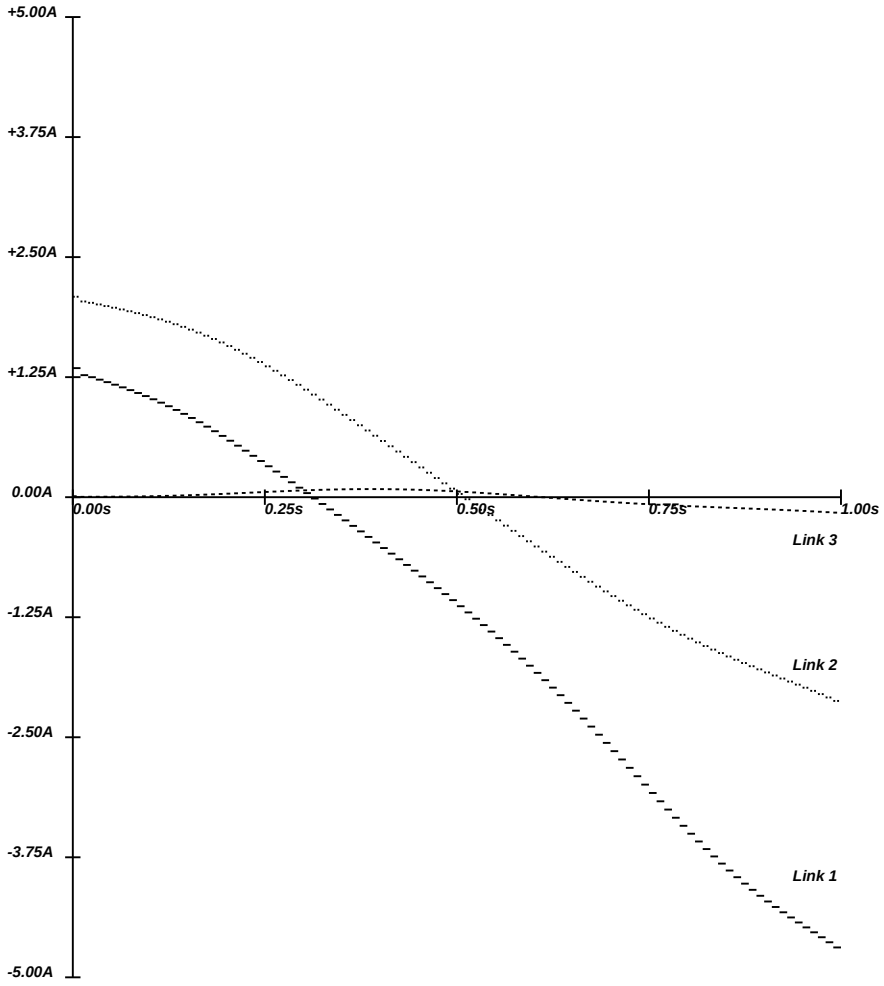

Figure 3: Current requirements to move a perfectly modeled finger from $\theta_i = 90°$ to $\theta_i = 0°$ in one second (gravity vector parallel to Y axis of palm) and an update frequency of 100Hz

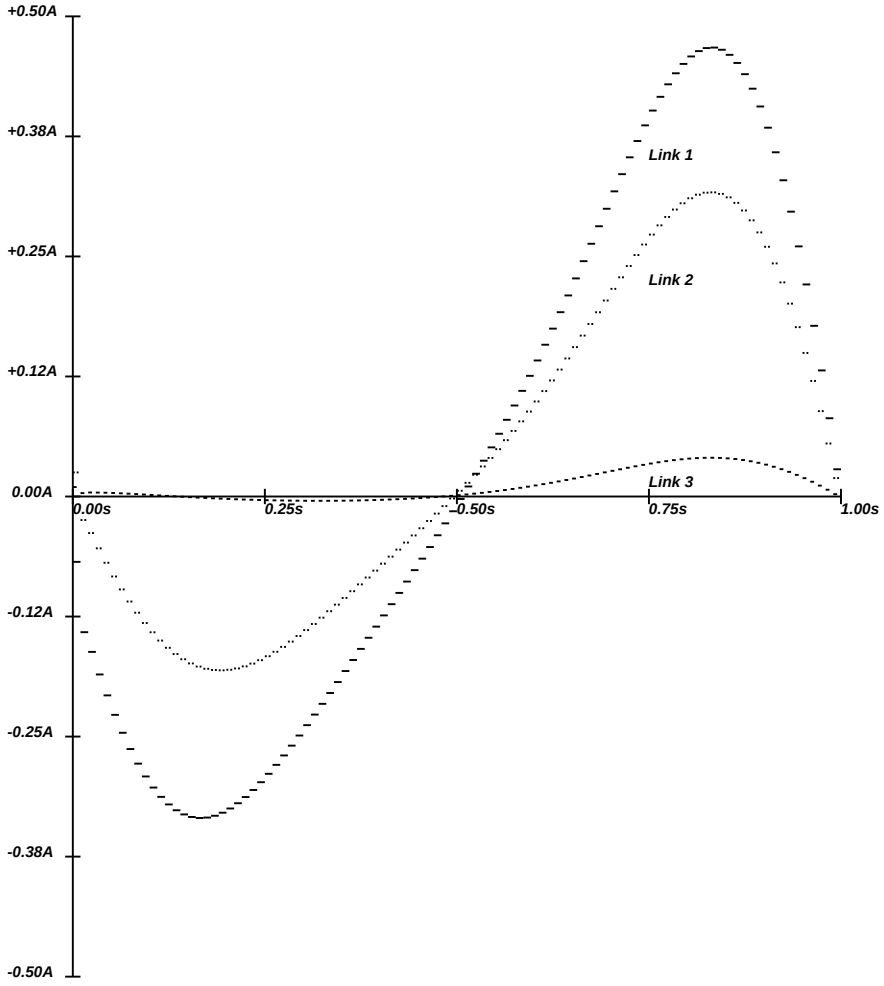

Figure 2: Current requirements to move a perfectly modeled finger from $\theta_i = 90°$ to $\theta_i = 0°$ in one second (gravity vector parallel to Z axis of palm) and an update frequency of 100Hz

which is shown in Figure 4 with the palm's Y axis parallel to the gravity vector. This trajectory does not use the full workspace of the hand to avoid irregularities at angles 0° and 90° where the joints reach their limits. The graph shows that the hand can be used at high speeds with little current in the given configuration.

This suggests that direct drive robot arms may be operated at lower currents if the natural swinging frequency is employed for pick and place operations. For instance a complete direct drive robot arm with a 3 dimensional workspace could let the arm swing instead of following a straight line from the pick up point to the put down point.

$$
\begin{aligned}
\ddot{\theta}(t) &= e_a(M^{-1}(\theta(t))\left[e_\tau(\tau) - V(\theta(t),\dot{\theta}(t)) - G(\theta(t))\right]) \\
\dot{\theta}(t+\Delta t) &= e_v(\dot{\theta}(t) + \ddot{\theta}(t)\Delta t) \\
\theta(t+\Delta t) &= e_p(\theta(t) + \dot{\theta}(t)\Delta t + \frac{1}{2}\ddot{\theta}(t)\Delta t^2)
\end{aligned}
$$

The complete system is shown in below.

$(*) \quad \rightarrow \quad \downarrow$

Trajectory generation:

$\theta_d(t) = a_0 + a_1 t + a_2 t^2 + a_3 t^3 + a_4 t^4 + a_5 t^5$

$\dot{\theta}_d(t) = a_1 + 2a_2 t + 3a_3 t^2 + 4a_4 t^3 + 5a_5 t^4$

$\ddot{\theta}_d(t) = 2a_2 + 6a_3 t + 12a_4 t^2 + 20a_5 t^3$

$\downarrow$

Control algorithm:

- Torque control

  $r_{ct}(\theta_d, \theta, \dot{\theta}_d, \dot{\theta}, \ddot{\theta}_d) = M(\theta)\ddot{\theta}^* + V(\theta, \dot{\theta}) + G(\theta)$

  with

  $\ddot{\theta}^* = \ddot{\theta}_d + K_v(\dot{\theta}_d - \dot{\theta}) + K_p(\theta_d - \theta)$

- Current control and check for maximum current requirement

  $I = \frac{\tau_{ct}(\theta_d, \theta, \dot{\theta}_d, \dot{\theta}, \ddot{\theta}_d)}{K_{Tmax} \cdot r(\theta) \cdot \sin(\theta + 45°)}$

$\downarrow$

Simulation

$\ddot{\theta}(t) = e_a(M^{-1}(\theta(t))\left[e_\tau(\tau) - V(\theta(t),\dot{\theta}(t)) - G(\theta(t))\right])$

$\dot{\theta}(t+\Delta t) = e_v(\dot{\theta}(t) + \ddot{\theta}(t)\Delta t)$

$\theta(t+\Delta t) = e_p(\theta(t) + \dot{\theta}(t)\Delta t + \frac{1}{2}\ddot{\theta}(t)\Delta t^2)$

$(*) \quad \hookleftarrow$

To simulate control of the hand we set the position gains $k_p = 1000$ and the velocity gains $k_v = 63.2$ which provided adequate stiffness as well as accurate control. Simulations have shown that the computed torque controller we implemented was stable for errors of up to 10% for accelerations and velocities and for errors of up to 5% for torques. Position errors of up to 2.5% gave reasonable results and should thus be measured with high accuracy.

The simulation program is also used to give us a graphical output of the current requirements during a trajectory. In Figure 2 the current requirements are shown for a finger which moves from $\theta_i = 90°$ to $\theta_i = 0°$ in one second for a perfectly modeled finger ($e_i = 0$) with the gravity vector parallel to the palm's Z axis. The same movement is shown in Figure 3 but this time the gravity vector is parallel to the palm's Y axis.

We also implemented a fast close hand/open hand trajectory

$$\theta(t) = \frac{85°}{2}(1 - \cos(360° \cdot \frac{3}{2} \cdot t)) + 2.5°$$

or

$$I = \frac{\tau_{ff}(\theta_d, \theta, \dot{\theta}_d, \dot{\theta}, \ddot{\theta}_d)}{K_{Tmax} \cdot r(\theta) \cdot \sin(\theta + 45°)}$$

We supply the required current to the coils using a H-bridge as seen in Figure 27 for every coil. The current to the H-bridge is controlled via pulse width modulation. The amount of current is proportional to the duty cycle of the signal at pin 5.

4.3 Simulation

In order to simulate the properties of the hand we implemented a 5^{th} order trajectory polynomial

$$\theta_d(t) = a_0 + a_1 t + a_2 t^2 + a_3 t^3 + a_4 t^4 + a_5 t^5$$

with the constraints

$$\begin{aligned} \dot{\theta}_0 &= 0 \\ \dot{\theta}_f &= 0 \\ \ddot{\theta}_0 &= 0 \\ \ddot{\theta}_f &= 0 \end{aligned}$$

where θ_o is the initial position and θ_f is the final position.

A 5^{th} order trajectory polynomial has an advantage over a 3^{rd} order polynomial because when the finger moves from $\theta_i = 0°$ to $\theta_i = 90°$ maximum accelerations occur at angles of $\theta = 6°$ and $\theta = 84°$ whereas for the 3^{rd} order polynomial calls for maximum accelerations at angles $\theta = 0°$ and $\theta = 90°$ where we have the least torque available.

The constants of the trajectory are given by

$$\begin{aligned} a_0 &= \theta_0 \\ a_1 &= 0 \\ a_2 &= 0 \\ a_3 &= \frac{10\theta_f - 10\theta_0}{t_f^3} \\ a_4 &= \frac{15\theta_0 - 15\theta_f}{t_f^4} \\ a_5 &= \frac{6\theta_f - 6\theta_0}{t_f^5} \end{aligned}$$

To simulate the dynamics of the hand we calculated the dynamics of the hand according to our model which included the error functions e_τ, e_a, e_v and e_p for torque, acceleration, velocity and position. The error functions e_τ, e_a, e_v give a random output that lies within a preset percentage of the input. The error function e_p changes the input for up to the preset percentage of 90°.

with

$$\ddot{\theta}^* = \ddot{\theta}_d + K_v(\dot{\theta}_d - \dot{\theta}) + K_p(\theta_d - \theta)$$

where

θ_d	is the desired position
$\dot{\theta}_d$	is the desired velocity
$\ddot{\theta}_d$	is the desired acceleration
θ	is the position measured with hall sensors
$\dot{\theta}$	is the velocity computed from sampled position data
K_p	is a 3×3 matrix with position gains k_p
K_v	is a 3×3 matrix with velocity gains k_v

For this controller we get the following error equation

$$\ddot{E} + K_v\dot{E} + K_pE = 0 \qquad \text{with} \qquad E = (\theta_d - \theta)$$

So we should make the gains k_p as large as possible in order to achieve high stiffness and a small steady state error. In order to achieve an over damped system we have to choose

$$k_v = 2\sqrt{k_p}$$

According to An et al. [10] computed torque control and feed forward torque control both give comparable results. However it seems interesting to give experimental results on how computed torque control and feed forward torque control compare for miniature direct drive devices.

The feed forward torque control for the finger would be given by

$$\tau_{ff}(\theta_d, \dot{\theta}_d, \ddot{\theta}_d) = M(\theta)\ddot{\theta} + V(\theta, \dot{\theta}) + G(\theta) + K_v(\dot{\theta}_d - \dot{\theta}) + K_p(\theta_d - \theta)$$

This controller has the following error equation

$$\ddot{E} + M^{-1}(\theta)K_v\dot{E} + M^{-1}(\theta)K_pE = 0$$

So we need to choose

$$K_v = 2\sqrt{M(\theta)K_p}$$

in order to have complex roots at all times and thereby eliminating oscillation we should choose the gains according to

$$K_v \leq 2\min_{\theta}\sqrt{M(\theta)K_p}.$$

So we need to apply the following currents to the coils depending on which controller we choose:

$$I = \frac{\tau_{ct}(\theta_d, \theta, \dot{\theta}_d, \dot{\theta}, \ddot{\theta}_d)}{K_{Tmax} \cdot r(\theta) \cdot \sin(\theta + 45°)}$$

4 Hand control

4.1 Direct drive actuator control

The torque of a magnetic moment inside a magnetic field is given by

$$\tau = B \times \mu$$

In our case let the magnet inside the magnet part of a link have the magnetic moment μ and the coils around the joints create a magnetic field B. Thus we control the torque to the joints by changing the magnetic field created by the joints. We can rewrite the above equation as

$$\tau = |B| \cdot |\mu| \cdot \sin(\theta + 45^\circ) \qquad \theta = 0^\circ \ldots 90^\circ$$

The magnetic field created by a coil is proportional to the current flowing through the windings of the coil and can be approximated by

$$B = \mu_0 \mu_r \frac{n}{l} I$$

So the torque exerted on the magnet inside a uniform magnetic field as a function of current is given by

$$\tau = K_{Tmax} \cdot I \cdot \sin(\theta + 45^\circ)$$

where K_{Tmax} is the torque constant at the maximum.

However since our coils do not produce a uniform magnetic field, we have to include a scaling function to describe the torque as a function of I.

$$\tau = K_{Tmax} \cdot I \cdot r(\theta) \cdot \sin(\theta + 45^\circ)$$

In the case of our actuator we can approximate the function $r(\theta)$ with

$$r(\theta) = \sin(\theta + 45^\circ)$$

as suggested by David Max which gives a relatively close approximation as seen from Figure 6, where the dashed line shows the function $K_{Tmax} \cdot \sin^2(\theta + 45^\circ)$. Depending on the uniformity of the actuators used in the different links, we might consider a different scaling function for each link.

4.2 Finger control

Now that we have the the torque as a function of current we are ready to implement a control algorithm for one finger. We chose a computed torque controller given by

$$\tau_{ct}(\theta_d, \theta, \dot{\theta}_d, \dot{\theta}, \ddot{\theta}_d) = M(\theta)\ddot{\theta}^* + V(\theta, \dot{\theta}) + G(\theta)$$

$$
\begin{aligned}
M_{12} &= m_2(a_1 r_{C_2} c_2 + r_{C_2}^2) + I_{zz2} + m_3(a_2^2 + r_{C_3}^2 + a_1 a_2 c_2 + a_1 r_{C_3} c_{23} + 2a_2 r_{C_3} c_3) + I_{zz3} \\
M_{13} &= m_3(r_{C_3}^2 + a_1 r_{C_3} c_{23} + a_2 r_{C_3} c_3) + I_{zz3} \\
M_{21} &= m_2(a_1 r_{C_2} c_2 + r_{C_2}^2) + I_{zz2} + m_3(a_2^2 + r_{C_3}^2 + a_1 a_2 c_2 + a_1 r_{C_3} c_{23} + 2a_2 r_{C_3} c_3) + I_{zz3} \\
M_{22} &= m_2 r_{C_2}^2 + I_{zz2} + m_3(a_2^2 + r_{C_3}^2 + 2a_2 r_{C_3} c_3) + I_{zz3} \\
M_{23} &= m_3(r_{C_3}^2 + a_2 r_{C_3} c_3) + I_{zz3} \\
M_{31} &= m_3(r_{C_3}^2 + a_1 r_{C_3} c_{23} + a_2 r_{C_3} c_3) + I_{zz3} \\
M_{32} &= m_3(r_{C_3}^2 + a_2 r_{C_3} c_3) + I_{zz3} \\
M_{33} &= m_3 r_{C_3}^2 + I_{zz3}
\end{aligned}
$$

$$
\begin{aligned}
V_1 &= (-2m_2 a_1 r_{C_2} s_2 - 2m_3 a_1 a_2 s_2 - 2m_3 a_1 r_{C_3} s_{23})\dot{\theta}_1\dot{\theta}_2 \\
&\quad +(-2m_3 a_1 r_{C_3} s_{23} - 2m_3 a_2 r_{C_3} s_3)\dot{\theta}_1\dot{\theta}_3 \\
&\quad +(-m_2 a_1 r_{C_2} s_2 - m_3 a_1 a_2 s_2 - m_3 a_1 r_{C_3} s_{23})\dot{\theta}_2^2 \\
&\quad +(-2m_3 a_1 r_{C_3} s_{23} - 2m_3 a_2 r_{C_3} s_3)\dot{\theta}_2\dot{\theta}_3 \\
&\quad +(-m_3 a_1 r_{C_3} s_{23} - m_3 a_2 r_{C_3} s_3)\dot{\theta}_3^2 \\
V_2 &= (m_2 a_1 r_{C_2} s_2 + m_3(a_1 a_2 s_2 + a_1 r_{C_3} s_{23}))\dot{\theta}_1^2 \\
&\quad -2m_3 a_2 r_{C_3} s_3 \dot{\theta}_1\dot{\theta}_3 \\
&\quad -2m_3 a_2 r_{C_3} s_3 \dot{\theta}_2\dot{\theta}_3 \\
&\quad -m_3 a_2 r_{C_3} s_3 \dot{\theta}_3^2 \\
V_3 &= m_3(a_1 r_{C_3} s_{23} + a_2 r_{C_3} s_3)\dot{\theta}_1^2 \\
&\quad +2m_3 a_2 r_{C_3} s_3 \dot{\theta}_1\dot{\theta}_2 \\
&\quad +m_3 a_2 r_{C_3} s_3 \dot{\theta}_2^2
\end{aligned}
$$

$$
\begin{aligned}
G_1 &= m_1(g_x r_{C_1} s_1 - g_y r_{C_1} c_1) \\
&\quad +m_2(g_x(a_1 s_1 + r_{C_2} s_{12}) - g_y(a_1 c_1 + r_{C_2} c_{12})) \\
&\quad +m_3(g_x(a_1 s_1 + a_2 s_{12} + r_{C_3} s_{123}) - g_y(a_1 c_1 + a_2 c_{12} + r_{C_3} c_{123})) \\
G_2 &= m_2(g_x r_{C_2} s_{12} - g_y r_{C_2} c_{12}) + m_3(g_x(a_2 s_{12} + r_{C_3} s_{123}) - g_y(a_2 c_{12} + r_{C_3} c_{123})) \\
G_3 &= m_3(g_x r_{C_3} s_{123} - g_y r_{C_3} c_{123})
\end{aligned}
$$

We now compute the partial derivatives involved.

$$\begin{aligned}
\frac{\partial k}{\partial \dot{\theta}_1} &= (m_1 r_{C_2}^2 + I_{zz1} + m_2(a_1^2 + 2a_1 r_{C_2} c_2 + r_{C_2}^2) + I_{zz2})\dot{\theta}_1 \\
&\quad +(m_3(a_1^2 + a_2^2 + r_{C_3}^2 + 2a_1 a_2 c_2 + 2a_1 r_{C_3} c_{23} + 2a_2 r_{C_3} c_3) + I_{zz3})\dot{\theta}_1 \\
&\quad +(m_2(a_1 r_{C_2} c_2 + r_{C_2}^2) + I_{zz2} + m_3(a_2^2 + r_{C_3}^2 + a_1 a_2 c_2 + a_1 r_{C_3} c_{23} + 2a_2 r_{C_3} c_3) + I_{zz3})\dot{\theta}_2 \\
&\quad +(m_3(r_{C_3}^2 + a_1 r_{C_3} c_{23} + a_2 r_{C_3} c_3) + I_{zz3})\dot{\theta}_3 \\
\frac{\partial k}{\partial \dot{\theta}_2} &= (m_2(a_1 r_{C_2} c_2 + r_{C_2}^2) + I_{zz2} + m_3(a_2^2 + r_{C_3}^2 + a_1 a_2 c_2 + a_1 r_{C_3} c_{23} + 2a_2 r_{C_3} c_3) + I_{zz3})\dot{\theta}_1 \\
&\quad +(m_2 r_{C_2}^2 + I_{zz2} + m_3(a_2^2 + r_{C_3}^2 + 2a_2 r_{C_3} c_3) + I_{zz3})\dot{\theta}_2 \\
&\quad +(m_3(r_{C_3}^2 + a_2 r_{C_3} c_3) + I_{zz3})\dot{\theta}_3 \\
\frac{\partial k}{\partial \dot{\theta}_3} &= (m_3(r_{C_3}^2 + a_1 r_{C_3} c_{23} + a_2 r_{C_3} c_3) + I_{zz3})\dot{\theta}_1 \\
&\quad +(m_3(r_{C_3}^2 + a_2 r_{C_3} c_3) + I_{zz3})\dot{\theta}_2 \\
&\quad +(m_3 r_{C_3}^2 + I_{zz3})\dot{\theta}_3
\end{aligned}$$

$$\begin{aligned}
\frac{\partial k}{\partial \theta_1} &= 0 \\
\frac{\partial k}{\partial \theta_2} &= -m_2 a_1 r_{C_2} s_2 \dot{\theta}_1(\dot{\theta}_1 + \dot{\theta}_2) + m_3(-a_1 a_2 s_2 \dot{\theta}_1(\dot{\theta}_1 + \dot{\theta}_2) - a_1 r_{C_3} s_{23} \dot{\theta}_1(\dot{\theta}_1 + \dot{\theta}_2 + \dot{\theta}_3)) \\
\frac{\partial k}{\partial \theta_3} &= m_3(-a_1 r_{C_3} s_{23} \dot{\theta}_1(\dot{\theta}_1 + \dot{\theta}_2 + \dot{\theta}_3) - a_2 r_{C_3} s_3(\dot{\theta}_1 + \dot{\theta}_2)(\dot{\theta}_1 + \dot{\theta}_2 + \dot{\theta}_3))
\end{aligned}$$

$$\begin{aligned}
\frac{\partial u}{\partial \theta_1} &= m_1(g_x r_{C_1} s_1 - g_y r_{C_1} c_1) \\
&\quad +m_2(g_x(a_1 s_1 + r_{C_2} s_{12}) - g_y(a_1 c_1 + r_{C_2} c_{12})) \\
&\quad +m_3(g_x(a_1 s_1 + a_2 s_{12} + r_{C_3} s_{123}) - g_y(a_1 c_1 + a_2 c_{12} + r_{C_3} c_{123})) \\
\frac{\partial u}{\partial \theta_2} &= m_2(g_x r_{C_2} s_{12} - g_y r_{C_2} c_{12}) + m_3(g_x(a_2 s_{12} + r_{C_3} s_{123}) - g_y(a_2 c_{12} + r_{C_3} c_{123})) \\
\frac{\partial u}{\partial \theta_3} &= m_3(g_x r_{C_3} s_{123} - g_y r_{C_3} c_{123})
\end{aligned}$$

We can write the torque at the joints as

$$\tau = M(\theta)\ddot{\theta} + V(\theta, \dot{\theta}) + G(\theta)$$

with

$$\begin{aligned}
M_{11} &= m_1 r_{C_2}^2 + I_{zz1} + m_2(a_1^2 + a_1 r_{C_2} c_2 + r_{C_2}^2) + I_{zz2} \\
&\quad +m_3(a_1^2 + a_2^2 + r_{C_3}^2 + 2a_1 a_2 c_2 + 2a_1 r_{C_3} c_{23} + 2a_2 r_{C_3} c_3) + I_{zz3}
\end{aligned}$$

be the total potential energy of one finger, where u_i is the potential of one finger link

$$\begin{aligned} u_i &= -m_i {}^0g^T {}^0P_{C_i} \\ \text{where} \quad {}^0g &= \begin{bmatrix} g_x \\ g_y \\ g_z \end{bmatrix} \end{aligned}$$

Thus we only consider the case in which the palm of the hand is stationary. This is a reasonable assumption to develop first control algorithms, since usually the hand is positioned with a robot arm and then performs some type of grasping operation during which the palm of the hand does not move. According to the orientation of the robot arm wrist, the vector ${}^0g$ can then be calculated. However if we were to make any grasping operations while moving the arm we would have to incorporate the dynamics of the arm as well.

The vectors that denote the position of the center of gravity of each link in the frame $\{0\}$ are given by:

$$\begin{aligned} {}^0P_{C_1} &= \begin{bmatrix} r_{C_1} c_1 \\ r_{C_1} s_1 \\ 0 \end{bmatrix} \\ {}^0P_{C_2} &= \begin{bmatrix} a_1 c_1 + r_{C_2} c_{12} \\ a_1 s_1 + r_{C_2} s_{12} \\ 0 \end{bmatrix} \\ {}^0P_{C_3} &= \begin{bmatrix} a_1 c_1 + a_2 c_{12} + r_{C_3} c_{123} \\ a_1 s_1 + a_2 s_{12} + r_{C_3} s_{123} \\ 0 \end{bmatrix} \end{aligned}$$

This gives us the potential energy as:

$$\begin{aligned} u_1 &= -m_1 (g_x r_{C_1} c_1 + g_y r_{C_1} s_1) \\ u_2 &= -m_2 (g_x (a_1 c_1 + r_{C_2} c_{12}) + g_y (a_1 s_1 + r_{C_2} s_{12})) \\ u_3 &= -m_3 (g_x (a_1 c_1 + a_2 c_{12} + r_{C_3} c_{123}) + g_y (a_1 s_1 + a_2 s_{12} + r_{C_3} s_{123})) \end{aligned}$$

The actuator torques are then given as

$$\tau = \frac{d}{dt} \frac{\partial L}{\partial \dot{\theta}} - \frac{\partial L}{\partial \theta}$$

with the Lagrangian

$$L(\theta, \dot{\theta}) = k(\theta, \dot{\theta}) - u(\theta)$$

$$+\left(\frac{1}{3}a_i^2+\frac{1}{6}h_{Ci}^2+2d_i^2+\left(r_{C_i}-l_i\right)^2\right)m_{Ci}$$

$$I_{zz3} = \left(\frac{1}{4}r_{M3}^2+\frac{1}{12}h_{M3}^2+r_{C_3}^2\right)m_{M3}+\left(\frac{1}{2}r_{T3}^2+\frac{1}{12}h_{T3}^2+\left(r_{C_3}-\frac{1}{2}h_{T3}\right)^2\right)m_{T3}$$

3.2 Dynamic equations

To calculate the dynamic equations of the finger we use the Lagrangian dynamic formulation. Let

$$k=\sum_i k_i$$

be the total energy of one finger, where k_i is the kinetic energy of one finger link

$$k_i=\frac{1}{2}m_i{}^0v_{C_i}^T{}^0v_{C_i}+\frac{1}{2}{}^iw_i^{TC_i}I_i{}^iw_i$$

and frame C_i has its origin at the center of mass of link i and has the same orientation as the frame {i}.

The velocities ${}^0v_{C_i}$ are given as follows:

$${}^0v_{C_1} = \begin{bmatrix} -r_{C_1}s_1\dot{\theta}_1 \\ r_{C_1}c_1\dot{\theta}_1 \\ 0 \end{bmatrix}$$

$${}^0v_{C_2} = \begin{bmatrix} -a_1s_1\dot{\theta}_1-r_{C_2}s_{12}(\dot{\theta}_1+\dot{\theta}_2) \\ a_1c_1\dot{\theta}_1+r_{C_2}c_{12}(\dot{\theta}_1+\dot{\theta}_2) \\ 0 \end{bmatrix}$$

$${}^0v_{C_3} = \begin{bmatrix} -a_1s_1\dot{\theta}_1-a_2s_{12}(\dot{\theta}_1+\dot{\theta}_2)-r_{C_3}s_{123}(\dot{\theta}_1+\dot{\theta}_2+\dot{\theta}_3) \\ a_1c_1\dot{\theta}_1+a_2c_{12}(\dot{\theta}_1+\dot{\theta}_2)+r_{C_3}c_{123}(\dot{\theta}_1+\dot{\theta}_2+\dot{\theta}_3) \\ 0 \end{bmatrix}$$

So the links of the finger have a kinetic energy as follows:

$$k_1 = \frac{1}{2}m_1r_{C_1}^2\dot{\theta}_1^2+\frac{1}{2}I_{zz1}\dot{\theta}_1^2$$

$$k_2 = \frac{1}{2}m_2\left(a_1^2\dot{\theta}_1^2+2a_1r_{C_2}c_2\dot{\theta}_1(\dot{\theta}_1+\dot{\theta}_2)+r_{C_2}^2(\dot{\theta}_1+\dot{\theta}_2)^2\right)+\frac{1}{2}I_{zz2}(\dot{\theta}_1+\dot{\theta}_2)^2$$

$$\begin{aligned} k_3 = {} & \frac{1}{2}m_3\left(a_1^2\dot{\theta}_1^2+a_2^2(\dot{\theta}_1+\dot{\theta}_2)^2+r_{C_3}^2(\dot{\theta}_1+\dot{\theta}_2+\dot{\theta}_3)^2+2a_1a_2c_2\dot{\theta}_1(\dot{\theta}_1+\dot{\theta}_2)\right) \\ & +m_3\left(a_1r_{C_3}c_{23}\dot{\theta}_1(\dot{\theta}_1+\dot{\theta}_2+\dot{\theta}_3)+a_2r_{C_3}c_3(\dot{\theta}_1+\dot{\theta}_2)(\dot{\theta}_1+\dot{\theta}_2+\dot{\theta}_3)\right) \\ & +\frac{1}{2}I_{zz3}(\dot{\theta}_1+\dot{\theta}_2+\dot{\theta}_3)^2 \end{aligned}$$

Let

$$u=\sum_i u_i$$

are the center of mass for each link and the zz-entry of the inertia tensor in order to achieve a more precise control. However no link can ever be precisely manufactured. Thus small inaccuracies remain. We feel that the larger and complexer a robot device gets, the more inaccuracies are introduced. An et al. [10] have devised a on-line method to derive the Denavit-Hartenberg parameters of a robot manipulator and the Inertia matrix of the links with only a few movements of the manipulator. It seems interesting to compare the level of errors of a conventional robot arm to those of a miniature robot device using the methods described by An et al.

	Link 1	Link 2	Link 3
r_{Mi} (cm)	0.7	0.7	0.7
h_{Mi} (cm)	3.5	2.9	2.1
r_{Ti} (cm)	0.7	0.7	0.7
h_{Ti} (cm)	4.0	4.0	5.5
h_{Ci} (cm)	0.8	0.8	0.8
a_i (cm)	2.25	2.25	2.25
b_i (cm)	1.5	1.5	1.5
d_i (cm)	0.7	0.7	0.7
l_i (cm)	6.0	6.0	6.0
m_{Mi} (g)	38.0	32.0	25.0
m_{Ti} (g)	4.5	4.5	6.2
m_{Ci} (g)	29.0	20.0	0.0
m_i (g)	100.5	76.5	31.2
r_{Ci} (cm)	3.55	3.25	0.546
I_{zzi} (kgm^2)	$7.95 \cdot 10^{-5}$	$5.85 \cdot 10^{-5}$	$6.70 \cdot 10^{-6}$

The center of mass is calculated as

$$\begin{aligned} \mathbf{r}_C &= \frac{1}{M}\int \mathbf{r}\,dm \\ r_{C_i} &= \frac{2l_i m_{Ci} + \frac{1}{2}h_{Ti}m_{Ti}}{m_i} \qquad i = 1,2 \\ \text{with} \quad m_i &= 2m_{Ci} + m_{Ti} + m_{Mi} \\ r_{C_3} &= \frac{\frac{1}{2}h_{T3}m_{T3}}{m_3} \\ \text{with} \quad m_3 &= m_{T3} + m_{M3} \end{aligned}$$

Since each finger is basically a planar manipulator we only need to consider the I_{zz} entry of each inertia matrix. If we place the parts according to Figure 1 we can calculate I_{zz} of the complete link using the parallel axis theorem as follows:

$$I_{zzi} = \left(\frac{1}{4}r_{Mi}^2 + \frac{1}{12}h_{Mi}^2 + r_{C_i}^2\right) m_{Mi} + \left(\frac{1}{2}r_{Ti}^2 + \frac{1}{12}h_{Ti}^2 + \left(r_{C_i} - \frac{1}{2}h_{Ti}\right)^2\right) m_{Ti}$$

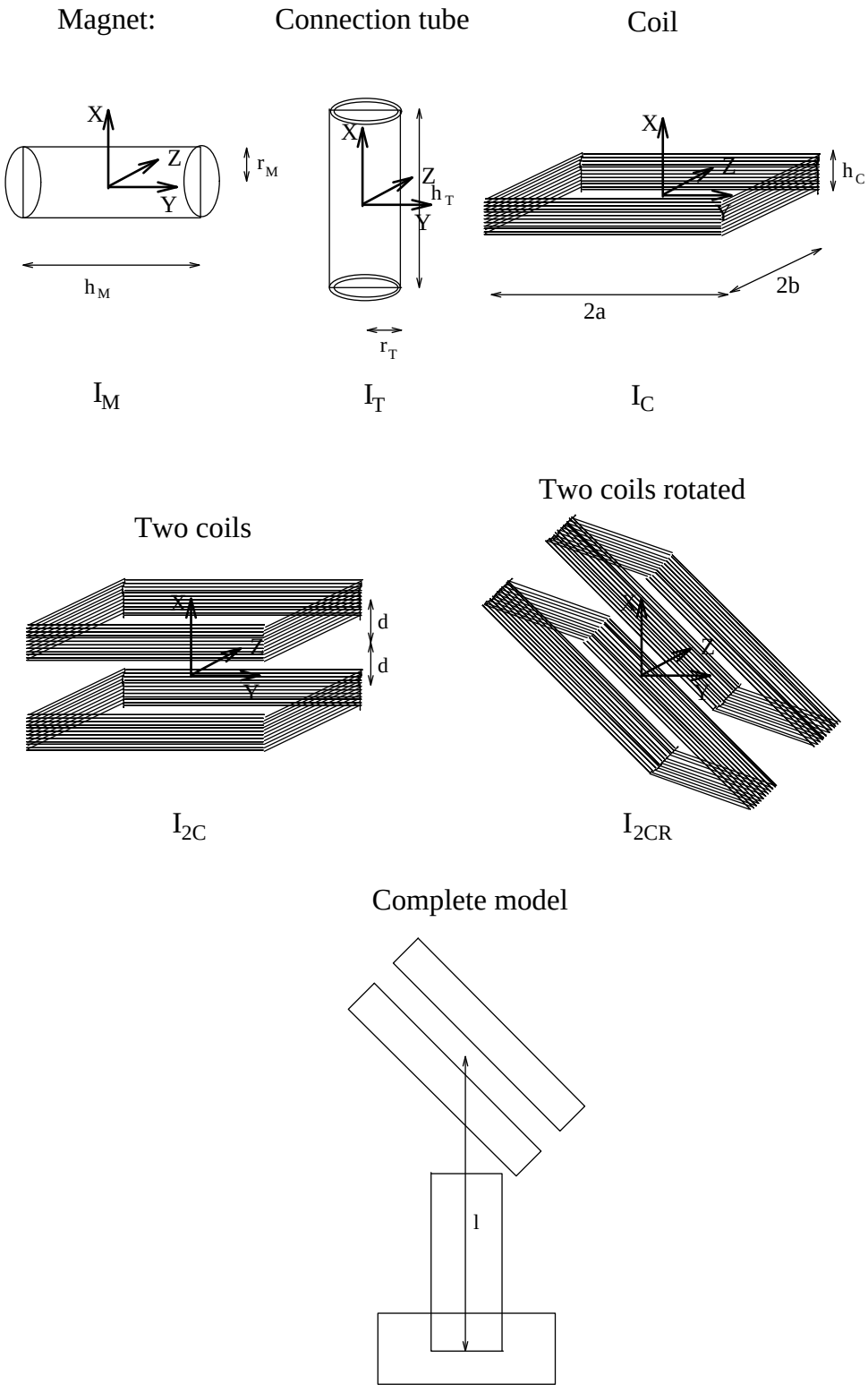

Figure 1: Inertia tensor model

- **Low cost** Brass is readily available and has a very low cost. Thus one has plenty material to work with and does not have to worry if a construction does not work out that well. One can simply start over.

Obviously if one wants to manufacture the direct drive hand in mass production, brass is not such a good choice any more, since the production process would simply take too long. Also it is inherently difficult do achieve a high precision hand using brass as an underlying material.

A possible solution to this problem would be to build the direct drive hand out of injection molded plastic. This could lead to high precision, stiffness of construction, fast assembly and also very low cost if there is a need for a large number of hands. With a precisely built hand it is furthermore possible to move the magnets closer to the coils and thereby increasing the strength of the hand.

3 Theory of operation

3.1 Inertia tensor model

We use the following approximation to model the inertia tensor. One finger link consists of a magnet tube, a connection tube and two coils as seen in Figure 1 with

$$I_M = \begin{pmatrix} \frac{1}{4}r_M^2 + \frac{1}{12}h_M^2 & 0 & 0 \\ 0 & \frac{1}{2}r_M^2 & 0 \\ 0 & 0 & \frac{1}{4}r_M^2 + \frac{1}{12}h_M^2 \end{pmatrix} m_M$$

$$I_T = \begin{pmatrix} r_T^2 & 0 & 0 \\ 0 & \frac{1}{2}r_T^2 + \frac{1}{12}h_T^2 & 0 \\ 0 & 0 & \frac{1}{2}r_T^2 + \frac{1}{12}h_T^2 \end{pmatrix} m_T$$

$$I_{2C} = \begin{pmatrix} \frac{1}{3}a^2 + \frac{1}{3}b^2 & 0 & 0 \\ 0 & \frac{1}{3}b^2 + \frac{1}{6}h_C^2 & 0 \\ 0 & 0 & \frac{1}{3}a^2 + \frac{1}{6}h_C^2 + 2d^2 \end{pmatrix} m_C$$

where

$$\begin{aligned} m_M &= \text{mass of magnet part} \\ m_T &= \text{mass of connection tube} \\ m_C &= \text{mass of one coil} \end{aligned}$$

As one can easily see from the modeling process and the dynamic equations below, a high degree of symmetry around the X axis is desirable. The better the model used, the more accurate the control algorithm will be. From the dynamic equations below we can see that in the case of a symmetric link the only two parameters to adjust

priced at about $3.50 each. Which added up to $292.50 for our hand. One micro controller such as the 68332 which is required for the computer control is priced at about $100 and increases thus the total cost of the hand to $400 (excluding any additional hardware and assembly time needed).

- **Overall Size** The overall size for the hand is quite small. The only other devices required other than the hand itself is the power supply and the control circuits. Tendon actuators are still quite large and occupy considerable space.
- **Dynamic model-based control** Since the hand can be operated at very high speeds the dynamics of the hand have to be modeled accurately in order to achieve precision control. Centripetal and coriolis terms may no longer be neglected. Model based control has already been successfully been implemented for direct drive devices.

However the direct drive hand also has its limitations:

- **Large Power Requirement** The power requirement for the hand is considerable. For our hand we require roughly 9kW to operate the hand at any orientation, which is way to much to operate the hand because of safety requirements and overheating in the coils, although further miniaturization would also decrease the power requirement.
- **Heat** The coils use for the hand heat up very fast due to the high power requirement. So the hand can only be operated for short periods of time with out overheating the coils. Needless to say that the hand may not be used in an environment were temperature needs to be precisely controlled (e.g. for laboratory experiments).
- **Low Torque** Since we still have the problem of overheating the coils to achieve high torque, the hand may only be operated with relatively low power. This in turn leads to low torque. The hand is not able to support itself if it is powered according to its heat constraints.

2 Design of Hand

The base material used in our design is brass. Brass has several advantages

- **Weight** Brass has a very light weight. To keep the total weight of the hand at a minimum was one of the major design points.
- **Ease of assembly** Brass is a material that is easy to work with yet stiff enough for our purposes. Also brass lets itself solder together very well.
- **Stiffness** Brass tubes resemble the bones in a human hand. These tubes are capable of enduring very strong forces without bending or losing of shape.

- **Long learning phase** A human operator first has to learn how to use a teleoperator. This learning experience can be quite long. It would be much easier if one could just use a data glove to control an artificial hand. The learning phase would be virtually eliminated. The operator only had to get comfortable with the look and feel of his new artificial hand.

This leads to

- **Low utilization** Since an existing teleoperator is quite different from a human hand, the operator constantly has to translate his natural way to handle objects into motions that are achievable with his teleoperator. If an operator could control an artificial hand then there would be no translation. The mapping would be one to one.

So if one had an artificial hand that resembles the human hand accurately in every way, these problems would be resolved. Apart from these problems, most existing teleoperators are very expensive high end products that are simple not usable in many cases due to economic reasons.

1.4 Advantages and limitations of a direct drive hand

The Utah/MIT Dextrous Hand and the Stanford Hand are very small, compact and very human like. Yet these hands have several drawbacks. Our hand employs miniature direct drive technology and thus is superior in the following points.

- **Response Time** Due to the direct drive actuators, the hand is able to respond virtually immediately to the instructions received by the controller. Once the correct positioning is calculated by an appropriate positioning algorithm, the hand can almost immediately be brought into the correct position.

- **Speed** As a result of the low response time, the hand is able to simulate the flexible, fast motions of the human hand quite accurately. This allows the simulation of many human abilities that require high speed motions such as playing a piano or typing at a keyboard.

- **Safety** An artificial hand that uses direct drive actuators does not pose a risk during human interaction. During operation, the links are still flexible and can give way to a human that is somehow entangled in the hand accidentally. Mechanical manipulators that use motors and gears for transmission of torque are usually locked in position and might not even release the object gripped even if turned off.

- **Low cost** Due to the use of inexpensive material the hand can be produced at very low cost. The brass material as well as any screws, nuts and the like used, adds up to roughly $20. For the complete hand one also needs 85 magnets

1.2 Background

In the past many different types of hands have already been developed. The Utah/MIT Dextrous Hand and the Stanford/JPL robot hand are probably the ones that are most widely known. The MIT hand, coming closest to the human hand in its appearance and range of motion, consists of 3 fingers and one thumb, whereas the Stanford hand consists of 3 rather all purpose fingers. Both of the hands use cables to actuate the finger joints. Tendon sensors are used to measure the tension of the wires.

A different approach was taken by the Belgrade/USC Hand [12] which does not maximize flexibility and dexterity. It has five fingers: a two jointed thumb and four three jointed fingers. The thumb can rotate about an axis parallel to the wrist. The hand was primarily developed for grasping tasks.

We refer the interested reader to Mason et al. [5] who give a more extensive survey about existing artificial hands.

1.3 Motivation and applications

Is there a need for an artificial human hand? An artificial hand can be used in a very large variety of environments. There are possible uses in environments that are otherwise inaccessible to a human being. For instance outer space is completely inaccessible to the human body if one wants to maintain the dexterity and flexibility of the human body. Astronauts are very limited in their ability to move because of their space suits that are still to thick to allow the same movements as one can do in a more friendly environment.

If it is possible to reduce the size of the hand, increases the torque it exerts and achieve all this with a low power consumption, then one could even use an artificial hand as a prosthetic extension for a human being that has lost his hand in an accident of some kind. Of course this would also require the development of an appropriate human/hand- interface.

In the near future one can also envision uses in workspaces in a factory that is inaccessible to humans due to poisonous gases or fumes. Here humans are endangered because they have to wear some kind of protective gear that might possibly fail. This is especially a big problem if a failure of such a protective gear is not immediately recognized and long term exposure to whatever hazards there are, permanently damages the human body.

Another area in which a direct drive hand could be employed would be in places of high radiation. Although radiation detectors are readily available a leak in a protective suit poses a severe health risk even when it is recognized because one has difficulty in closing it. An exposed person cannot simply put on a new suit in a contaminated environment. Recent nuclear reactor accidents have shown that indeed robotics devices such as an artificial human hand would be highly useful.

This also requires the development of appropriate teleoperation techniques. Existing teleoperators that do not resemble a human hand have two main problems:

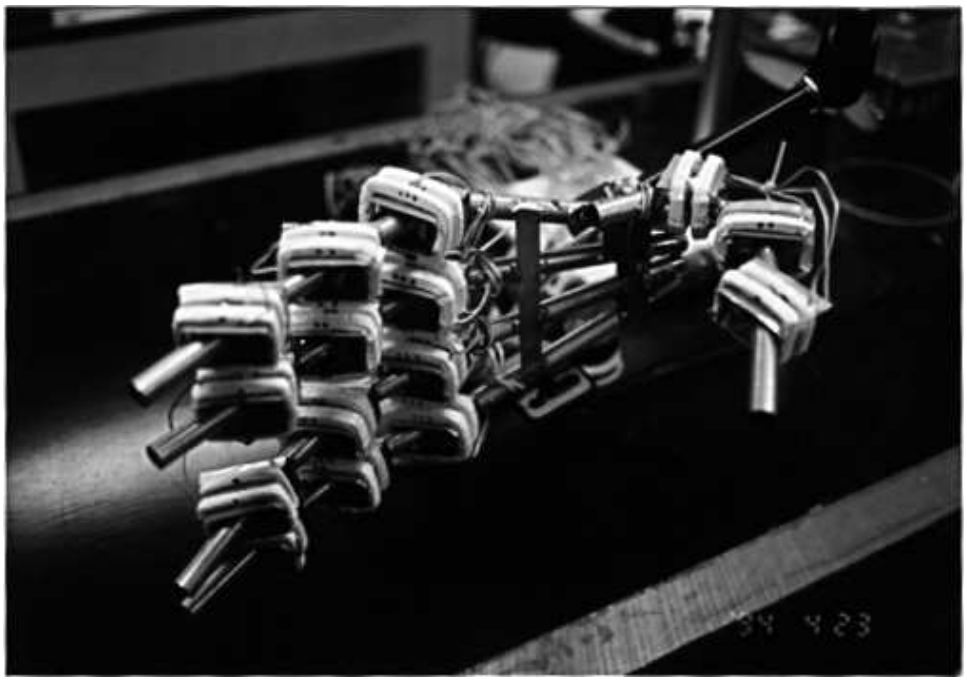

Abstract

An artificial 15 degrees of mobility direct drive hand, slightly bigger than a human hand, is presented. The underlying technology are the miniature direct drive actuators recently developed. The motivation for our design and the construction plan for the hand is given. The dynamics of the hand are analyzed theoretically and a model for control of the hand is presented. Finally we describe our experiences made while experimenting with the hand. A direct drive hand graphics interface has been developed to simulate the dynamics of the hand and to test out control algorithms for the hand.

1 Introduction

1.1 What is direct drive?

Direct drive means that the joints are moved directly by actuators which are physically aligned with the joint axis. There are no gears used for transmission of torque. Hence we drive the joints directly, without any intermediate transmission belts or similar devices. We drive our links by magnetic fields which are generated by coils that are wrapped around each and every joint. Several direct drive robots have already been successfully built although most of these robots were quite big. Because of the development of very powerful miniature neodymium iron boron (NdFeB) magnets it has become possible to miniaturize the direct drive technology.

Contents

A direct-drive hand: Design, Modeling and Control

Marc Ebner and Richard S. Wallace

June 30, 1994

Technical Report No. 66
Department of Computer Science
Courant Institute of Mathematical Sciences
New York University